薛宪法,邱昆峰,何登洋等. 2023. 西秦岭甘南早子沟石英闪长玢岩岩石成因及其地质意义. 岩石学报,39(02):463-483,doi:10.18654/1000-0569/2023.02.11

西秦岭甘南早子沟石英闪长玢岩岩石成因及其地质意义*

薛宪法[1]　邱昆峰[1**]　何登洋[1]　黄雅琪[1]　朱锐[2]　于皓丞[1]　姜桂鹏[2]

XUE XianFa[1], QIU KunFeng[1**], HE DengYang[1], HUANG YaQi[1], ZHU Rui[2], YU HaoCheng[1] and JIANG GuiPeng[2]

1. 中国地质大学(北京)地球科学与资源学院,北京　100083
2. 甘肃省合作早子沟金矿有限责任公司,招金矿业股份有限公司,合作　747000
1. *School of Earth Science and Resources, China University of Geosciences, Beijing* 100083, *China*
2. *Gansu Hezuo Zaozigou Gold Company, Zhaojin Mining Industry Co., Ltd., Hezuo* 747000, *China*

2022-09-01 收稿, 2022-12-21 改回.

Xue XF, Qiu KF, He DY, Huang YQ, Zhu R, Yu HC and Jiang GP. 2023. Petrogenesis of the quartz diorite porphyry in the Zaozigou, West Qinling and its geological implications. *Acta Petrologica Sinica*, 39(2): 463-483, doi: 10.18654/1000-0569/2023.02.11

Abstract　The West Qinling Orogenic Belt, located between the North China Block and the South China Block, is one of the most important gold regions in China. It records the evolution of the northeastern branch of the Paleo-Tethys in East Asia, which is of great significance for understanding the collision of the North China Block and the South China Block. Most of the Early-Middle Triassic igneous rocks are associated with the subduction process of the Mianlue Ocean, however, its closure time remains unclear. In present study, the zircon U-Pb geochronology, major- and trace-element geochemistry, and Lu-Hf isotopic analyses are employed to investigate the petrogenesis and geodynamic setting of the quartz diorite porphyry from the Zaozigou, and to constrain the closure time of the Mianlue Ocean. Zircon LA-ICP-MS U-Pb age suggests the quartz diorite porphyry intruded at ca. 232Ma, as the products of Middle Triassic magmatism. The quartz diorite porphyry is characterized by relatively high SiO_2 values (56.18% ~ 68.26%), high K_2O contents (1.82% ~ 3.70%) and intermediate A/CNK values (0.73 ~ 1.07). Their metaluminous to weakly peraluminous and potassium-rich characteristics reveal that the Triassic granitoids are generated by partial melting of a medium- to high-K mafic lower crust. Moreover, they are enriched in LREEs, depleted in HREEs, and characterized by negative Eu anomalies in the chondrite-normalized REE patterns, which is typical of continental crust rocks. The high $Mg^{\#}$ values (47.57 ~ 70.35) of the quartz diorite porphyry indicate the involvement of lithospheric mantle materials and/or magma mixing. The relatively wide ranges of $\varepsilon_{Hf}(t)$ from -12.9 to -7.12 and two-stage Hf model ages (1.70 ~ 2.10Ga) imply that the magma originated from partial melting of the Paleo-Proterozoic lower crust. We conclude that the quartz diorite porphyry was formed in the active continental margin, with characteristics of pre-collision granitic rock, and formed under the background of northward subduction of the Mianlue ocean crust, supporting that the Mianlue oceanic crust closed after ~232Ma.

Key words　Zircon U-Pb geochronology; Lu-Hf isotope; Whole-rock geochemistry; Zaozigou quartz diorite porphyry; West Qinling Orogen

摘　要　西秦岭造山带位于华北板块和华南板块之间,是我国中央造山带的重要组成部分,记录了东亚古特提斯洋东北支的演化历史,对于探讨华北板块和华南板块的碰撞过程具有重要意义。西秦岭广泛发育的早-中三叠世火成岩与勉略洋壳向

* 本文受国家自然科学基金项目(42072087、42261134535)、高等学校学科创新引智计划(BP0719021)、矿床地球化学国家重点实验室开放研究(202202)和北京市科技新星计划课题(Z201100006820097)联合资助.

第一作者简介: 薛宪法,男,1999 年生,硕士生,矿物学、岩石学、矿床学专业,E-mail: xianfa_xue@qq.com

** **通讯作者:** 邱昆峰,男,1986 年生,教授,博士生导师,从事矿床学教学与研究工作,E-mail: kunfengqiu@qq.com

北俯冲有关,但勉略洋壳的闭合时限仍有争议。因此本文对采自早子沟地区的石英闪长玢岩进行锆石 U-Pb 年代学、Lu-Hf 同位素和全岩主微量地球化学分析,查明早子沟石英闪长玢岩成因及其构造演化背景,并进一步约束勉略洋壳闭合时间。锆石 LA-ICP-MS U-Pb 定年结果表明,石英闪长玢岩侵位年龄为 ~232Ma,为中三叠世岩浆活动的产物。石英闪长玢岩含有较高的 SiO_2(56.18% ~68.26%),K_2O 为 1.82% ~3.70%,A/CNK 值为 0.73 ~1.07,是准铝质-弱过铝质的钙碱性-高钾钙碱性岩石。其富钾的特征,与中高钾基性下地壳部分熔融产生的熔体成分一致。轻重稀土分异明显,$(La/Yb)_N$ 比值为 8.10 ~61.2,富集大离子亲石元素(K、Sr、Ba、Cs),亏损高场强元素 Nb、Ta,具有弱负铕异常(δEu = 0.65 ~0.93),显示了典型的大陆地壳岩石特征。石英闪长玢岩较高的 $Mg^{\#}$ 值(47.57 ~70.35)意味着有一定幔源物质的加入。$\varepsilon_{Hf}(t)$ 在 -12.9 ~ -7.2 之间,对应的二阶段 Hf 模式年龄(t_{DM}^2)为 1.70 ~2.10Ga,表明岩浆来自于古元古代下地壳的重熔。本文认为石英闪长玢岩形成于勉略洋壳向北俯冲背景下的活动大陆边缘环境,具有碰撞前花岗质岩石特征,即勉略洋壳在 ~232Ma 仍处在俯冲阶段。

关键词 锆石 U-Pb 年代学;Lu-Hf 同位素;全岩地球化学;早子沟石英闪长玢岩;西秦岭造山带

中图法分类号 P588.134; P597.3

秦岭造山带呈带状分布于华北板块和华南板块之间,经历了前寒武纪基底演化、新元古代构造热事件、早古生代和三叠纪俯冲与碰撞四个重要的构造阶段,以及相应的大规模岩浆作用(Ren *et al.*, 2018; Wu *et al.*, 2018)。以徽成盆地和佛坪穹窿为界,秦岭造山带也被分为西秦岭造山带和东秦岭造山带,西秦岭造山带在区域上属于南秦岭造山带的一部分(Hu *et al.*, 2020)。西秦岭造山带位于秦岭-大别-苏鲁造山带西部,自元古代到中生代晚期,经历了多期次构造运动,导致其岩浆演化与东秦岭有巨大差异(Meng and Zhang, 2000; Deng *et al.*, 2017; Qiu *et al.*, 2018)。虽然秦岭造山带是由华北板块和华南板块碰撞形成,但西秦岭并未出现类似榴辉岩的超高压岩石(Dong and Santosh, 2016)。西秦岭基底岩性主要为新太古代英云闪长岩-奥长花岗岩-花岗闪长岩(TTG)组合(刘勇等,2012)和古元古代变质沉积序列(石英岩和大理岩)(裴先治等,2009),仅在天水地区沿西秦岭北缘零星出露。西秦岭造山带经历了三期变形事件:华北板块南侧的早-中古生代增生事件;沿勉略缝合带的晚古生代-三叠纪碰撞事件及华南板块与早期增生地体的拼合;侏罗纪至白垩纪的陆内造山作用(Li *et al.*, 2017; Qiu *et al.*, 2017; Deng *et al.*, 2022a, b)。

西秦岭地区三叠纪火成岩普遍形成于古特提斯洋向北俯冲(250 ~235Ma)的背景下,而后经历了华北板块和华南板块之间的同碰撞(228 ~215Ma)到碰撞后(215 ~185Ma)过程(Qiu *et al.*, 2017)。西秦岭地区东部的花岗质岩体多于 225 ~205Ma 发生侵位(Dong *et al.*, 2011),为过铝质-准铝质高钾钙碱性花岗质岩石,岩浆来源于华南板块中元古界的地壳熔融,可分为 228 ~215Ma(华北板块和华南板块陆陆碰撞背景下;Cao *et al.*, 2011; Zhu *et al.*, 2011)和 215 ~185Ma 两期岩浆事件(秦岭造山带由同碰撞向后碰撞的构造过渡时期;Xiao *et al.*, 2014; Xiong *et al.*, 2016)。西秦岭西部地区火成岩体侵位年龄约为 250 ~235Ma,多为弱过铝质-准铝质高钾钙碱性花岗质岩石,岩浆来源于(富钾)基性下地壳的部分熔融,但对于是否有幔源物质的参与仍有不同的认识(金维浚等, 2005; 骆必继等, 2012; 徐学义等, 2014; Qiu and Deng, 2017; 杨瀚文, 2018)。此外,西秦岭西部地区火成岩体形成的构造背景也存在争议,部分学者认为花岗质岩石是形成于活动大陆边缘环境,与勉略洋壳的消减作用有关(Li *et al.*, 2014; 黄雅琪等, 2020);但也有学者认为阿尼玛卿-勉略洋壳在晚二叠世发生闭合,西秦岭印支期花岗质岩石形成在陆-陆碰撞背景下(骆必继等, 2012; Xiong *et al.*, 2018)。

针对西秦岭西北缘花岗质岩石成因及构造演化问题,本文对西秦岭夏河-合作地区早子沟石英闪长玢岩开展了锆石 LA-ICP-MS U-Pb 年代学、锆石 Lu-Hf 同位素地球化学和全岩主微量元素分析工作,以探讨西秦岭地区花岗质岩石成因及地球动力学背景,并约束勉略洋壳闭合时限。

1 区域地质背景

秦岭造山带是我国中央造山带的重要组成部分,横跨中国中部,东西延伸 1500 多千米(图 1; 张国伟等, 2001; Deng and Wang, 2016; Qiu *et al.*, 2018; Deng *et al.*, 2020a, b)。秦岭造山带北以灵宝-鲁山-舞阳断裂和祁连造山带为界与华北板块相邻,南面以勉略-巴山-襄广断裂和松潘-甘孜造山带为界与华南板块相邻(图 1a; Yang *et al.*, 2015a, b; Deng *et al.*, 2017; Qiu *et al.*, 2021a)。秦岭造山带以宽坪缝合带、商丹缝合带和勉略缝合带从北向南划分为华北板块南缘、北秦岭板块、南秦岭板块和华南板块北缘(Yang *et al.*, 2015b; Qiu *et al.*, 2016a)。宽坪缝合带地处华北板块南缘与北秦岭板块之间,其广泛发育的蛇绿岩套主要由绿片岩和角闪岩相火山岩组成,形成于约 1.45 ~0.95Ga(Dong and Santosh, 2016; Dong *et al.*, 2016)。商丹缝合带位于北秦岭和南秦岭板块之间,主要出露古生代蛇绿岩套和与俯冲有关的火山岩及沉积岩(Dong *et al.*, 2016; Liu *et al.*, 2016)。位于南秦岭板块和华北板块北缘之间的勉略缝合带主要由不连续出露的蛇绿岩套、洋岛玄武岩和岛弧火山岩组成(Deng *et al.*, 2014; Yang *et al.*, 2016a)。华北板块南缘主要由前寒武纪基底和显生宙沉积盖层组成。基底主要为太古宙太华岩群,由黑云母斜长角闪岩、石英片岩和大理岩组成,上覆中元古代熊耳群、中元古代至新元古代海相沉积岩和新元古代冰碛

岩(Zhao *et al.*, 2004；时毓等，2011)。显生宙沉积岩主要为早古生代海相碎屑岩和碳酸盐岩及晚古生代至中生代陆相碎屑岩。元古宙秦岭群是北秦岭板块的主要基底岩层，由长英质片麻岩、角闪岩、石英片岩和大理岩组成，并被不连续出露的显生宙沉积地层覆盖(石炭系-三叠系陆相碎屑岩)(张国伟等，1996)。陡岭群和佛坪群是南秦岭板块的结晶基底，陡岭群由新太古代英云闪长岩-奥长花岗岩-花岗闪长岩(TTG)组合以及新元古代角闪岩、石英岩和大理石组成，元古代佛坪群由黑云母斜长岩、角闪岩、角闪片麻岩和混合岩组成(Hu *et al.*, 2013)。南秦岭板块上覆震旦纪海相碳酸盐岩和古生代沉积层序，包括寒武纪-奥陶纪灰岩、志留纪页岩和泥盆纪-石炭纪海相碎屑岩以及层间灰岩(Hu *et al.*, 2020；Wang *et al.*, 2020)。华南板块北缘结晶基底主要由新太古代-古元古代崆岭群组成，包括太古宙 TTG 组合和元古宙角闪岩、混合岩和变质碎屑岩(Deng *et al.*, 2022b；Yang *et al.*, 2022)，上覆震旦纪碎屑灰岩、寒武纪-奥陶纪灰岩、志留系纪-泥盆纪砂岩和粉砂岩、石炭纪-中三叠世碳酸盐岩和晚三叠世-白垩纪碎屑岩。

以徽成盆地和佛坪穹窿为界，秦岭造山带被分为东秦岭造山带和西秦岭造山带(Mao *et al.*, 2002；Dong *et al.*, 2011；Qiu and Deng, 2017)。西秦岭造山带长约 600km，是秦岭造山带的西延部分。该造山带经历了多期与古特提斯洋演化相关的构造事件以及随后的晚三叠世华北板块和华南板块的碰撞，是东古特提斯洋的分支(张国伟等，2001；Yu *et al.*, 2019；Xiao *et al.*, 2022)。区域内广泛出露泥盆纪至三叠纪沉积岩，而前寒武纪基底很少出露(Yang *et al.*, 2016b；Qiu *et al.*, 2021b)。西秦岭造山带岩浆活动频繁，尤其是中生代岩浆活动，并在印支期成矿作用中形成了许多金矿床(以造山型、岩浆热液型为主)，已探明的金储量超 1200t，是中国第二大金矿集区(Deng *et al.*, 2018, 2019；Goldfarb *et al.*, 2019；Yu *et al.*, 2020a, b, 2021；Huang *et al.*, 2022；Qiu *et al.*, 2023a, b)。夏河-合作地区位于西秦岭造山带的西北缘(图 1a)，区内主要出露石炭纪至三叠纪的海相沉积岩和早-中三叠世侵入岩，并含有少量二叠纪火山岩和白垩纪火山沉积岩(图 1b；梁志录等，2016；Xiao *et al.*, 2022)。区域北西向构造发育，以夏河-合作断裂及新堡-力士山背斜为主(梁志录等，2016；Sui *et al.*, 2017)。以夏河-合作断裂及其延长线为界，可分为北东和南西两个区域(韦良喜等，2018)，分别以与三叠纪花岗岩有密切时空关系的斑岩-矽卡岩型矿床和以发育脉状、浸染状的金锑矿床为主(Qiu *et al.*, 2018；Zhang *et al.*, 2021)。

2 矿床地质

早子沟金锑矿床位于甘肃合作市西南，大地构造位置位于西秦岭造山带西缘夏河-合作断裂南西方向(图 1b)，累计查明金资源量 106.2t，矿床平均品位 3.34g/t。早子沟金锑矿床赋矿围岩主要是下三叠统古浪堤组和三叠纪岩浆岩(图 2)。古浪堤组是矿区主要出露地层，约占矿区总面积的 70%，主要由硅质板岩、钙质板岩、石英砂岩和粉砂岩组成(刘勇，2012；隋吉祥和李建威，2013)。早-中三叠世岩浆岩呈岩脉、岩枝状侵入到早三叠世板岩内，呈北东和北北东向分布，主要的岩性为石英闪长玢岩、英安玢岩、闪长玢岩、流纹斑岩和花岗闪长玢岩。早子沟金锑矿床中金矿体分布明显受构造控制，按照矿体几何特征和控矿断裂性质，可将其分为两类：陡倾斜矿体和缓倾斜矿体(Qiu *et al.*, 2020；Yu *et al.*, 2022a)。陡倾斜矿体主要赋存在北东-北东东走向、陡倾斜的断裂带中，围岩为变形、碎裂的蚀变板岩和英安玢岩，主要矿石类型为浸染状英安玢岩和板岩矿石；缓倾斜矿体主要赋存在北北西走向、缓倾斜的断裂带内，围岩多为碎裂的蚀变板岩和英安玢岩，矿石类型主要为呈透镜体状产于断裂带内的石英-辉锑矿脉矿石。矿区多发育强烈的毒砂化、黄铁矿化、硅化、辉锑矿化和绢云母化。

3 样品描述及分析方法

石英闪长玢岩样品均采自早子沟矿区的野外露头(定年样品 18ZZG16 位置：34°57′55.30″N、102°48′27.52″E；样品 18ZZG17 位置：34°57′58.39″N、102°48′37.25″E)。样品呈灰黑色，块状构造，斑状结构，肉眼可见石英颗粒及少量较大颗粒的暗色矿物(黑云母和角闪石)(图 3)。斑晶(~50%)主要为斜长石(~25%)、石英(~15%)、黑云母(~5%)和角闪石(~5%)。斜长石和石英斑晶粒径多在 0.2~1mm 之间，最大可达 5mm，少量石英发育溶蚀结构。黑云母和角闪石斑晶大多在 0.2~0.3mm 之间。斜长石和石英多呈板状，黑云母呈自形片状，角闪石呈自形柱状。基质呈隐晶质结构，由斜长石(15%~30%)、石英(5%~25%)和少量副矿物(锆石和磷灰石)组成。

将石英闪长玢岩样品粉碎至 80~120 目，并通过电磁和重液分离技术分离锆石晶体。在双目显微镜下手工挑选锆石颗粒，将其安装在环氧树脂中，抛光至近一半以暴露内部结构，然后在含有 5% HNO_3 的超声波清洗机中清洗。在分析之前，使用 JXA-8800 电子探针和图像分析软件，在 20kV 和 20nA 条件下，获得锆石阴极发光(CL)图像，来观察锆石颗粒的内部结构。该工作在华北地质科技创新中心研究所完成。

锆石 LA-ICP-MS U-Pb 定年分析工作在华北地质科技创新中心同位素实验室进行。使用 Neptune 双聚焦多收集器 ICP-MS 进行激光采样，测试激光束斑直径为 30μm、频率为 8Hz。GJ-1 用作锆石 U-Pb 定年分析的标样。使用 NIST SRM 610 玻璃作为外标，计算锆石的 U、Th 和 Pb 浓度。同位素比值使用 ICPMSDataCal 11.8(Liu *et al.*, 2010)计算，并使用 Isoplot 3.0 版软件绘制锆石年龄协和图(Ludwig, 2003)。使用 Andersen (2002)的方法进行了普通 Pb 校正，详细实验方

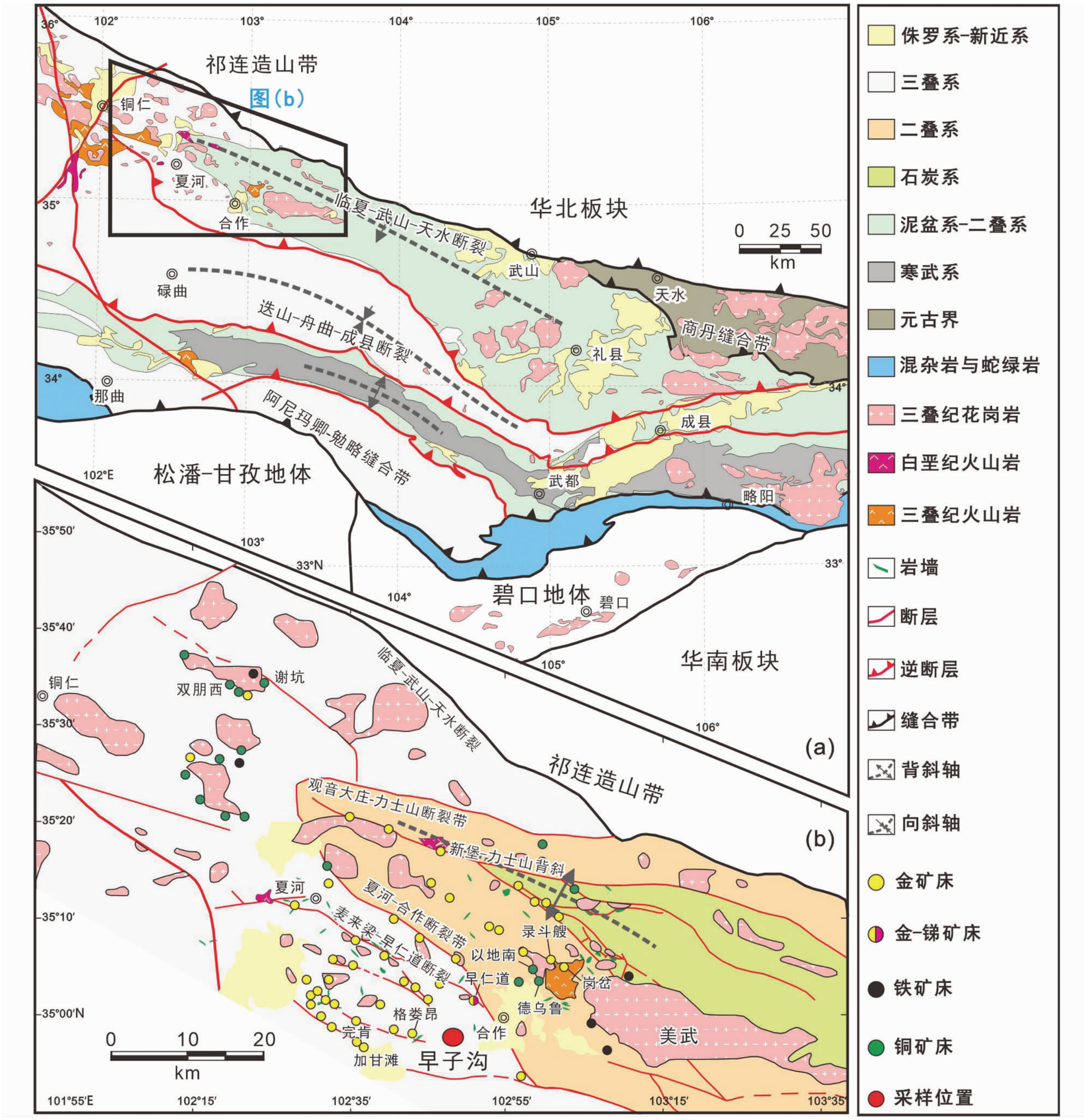

图1 西秦岭造山带地质简图(a)和夏河-合作地区地质简图及矿床分布图(b)(据 Qiu and Deng, 2017; Qiu *et al.*, 2020)

Fig. 1 Simplified geological map of the West Qinling Orogenic Belt in China (a) and simplified geological map of the Xiahe-Hezuo polymetallic district, showing the distribution of the Triassic granitoids and ore deposits (b) (after Qiu and Deng, 2017; Qiu *et al.*, 2020)

法见文献(Qiu *et al.*, 2019)。

在 U-Pb 年龄测试相同的位置上对样品进行锆石 Lu-Hf 同位素分析,该项工作在华北地质科技创新中心同位素实验室完成。使用与 UP 193nm 激光烧蚀系统耦合的 Thermo-Finnigan-Neptune MC-ICP-MS 系统测定 Hf 同位素组成。使用 11Hz、10J/cm^2 的激光重复烧蚀锆石,束斑直径为 50μm。在分析过程中,GJ-1 锆石标样的^{176}Hf/^{177}Hf 比值为 0.282009 ±24(2σ, n=13)(Elhlou *et al.*, 2006)。^{176}Lu 的衰变系数为 1.865×10^{-11}/yr,使用^{176}Hf/^{177}Hf = 0.282785 ± 11(2σ)和^{176}Hf/^{177}Hf = 0.0336 ± 1(2σ)的球粒陨石比值来计算 $\varepsilon_{Hf}(t)$ 的值(Blichert-Toft and Albarède, 1997)。

全岩主量分析在华北地质科技创新中心测定。把 1g 样品烘干后于 1000℃ 的高温炉中灼烧测得其烧失量(LOI)。取 0.5g 样品溶于 4g $Li_2B_4O_7$ 溶剂中,均匀混合后再加入

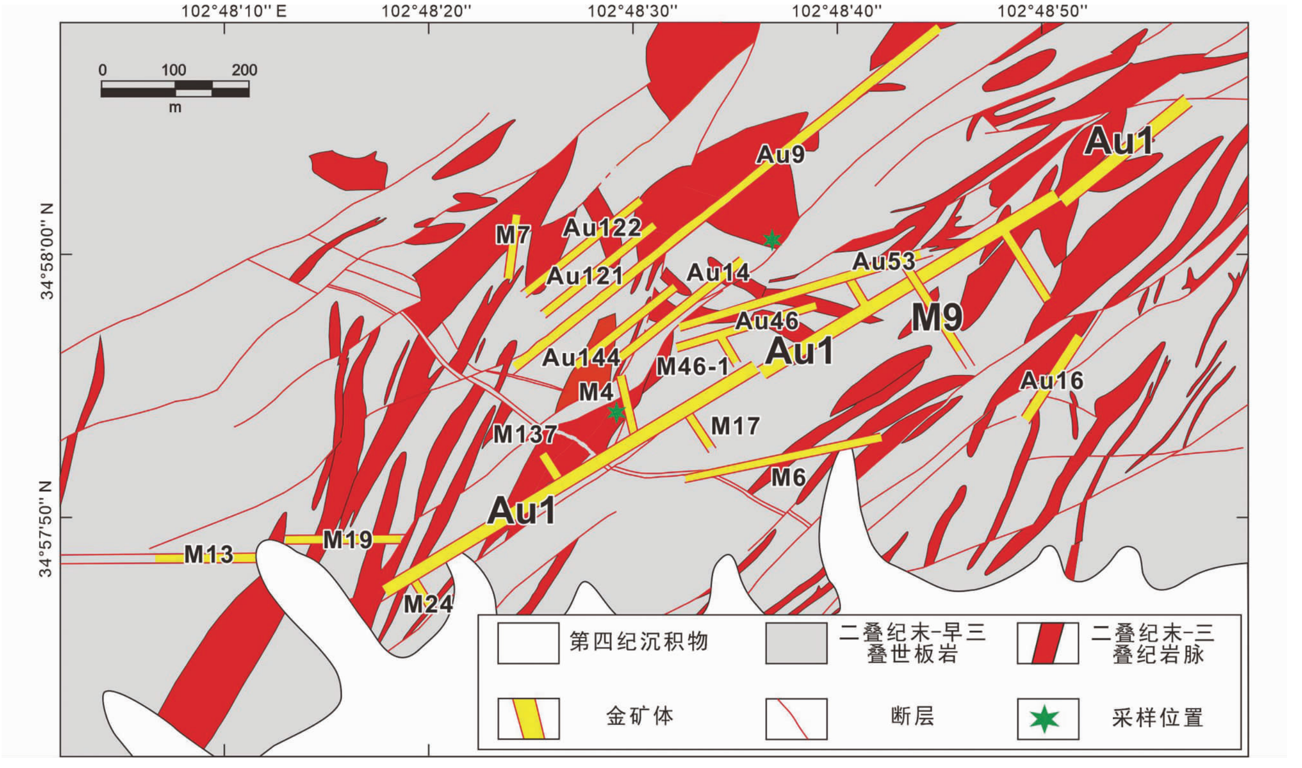

图 2 西秦岭早子沟金锑矿床地质简图(据 Yu *et al.*, 2019)

Fig. 2 Sketch geologic map of the giant Zaozigou Au-Sb deposit in the West Qinling, China (after Yu *et al.*, 2019)

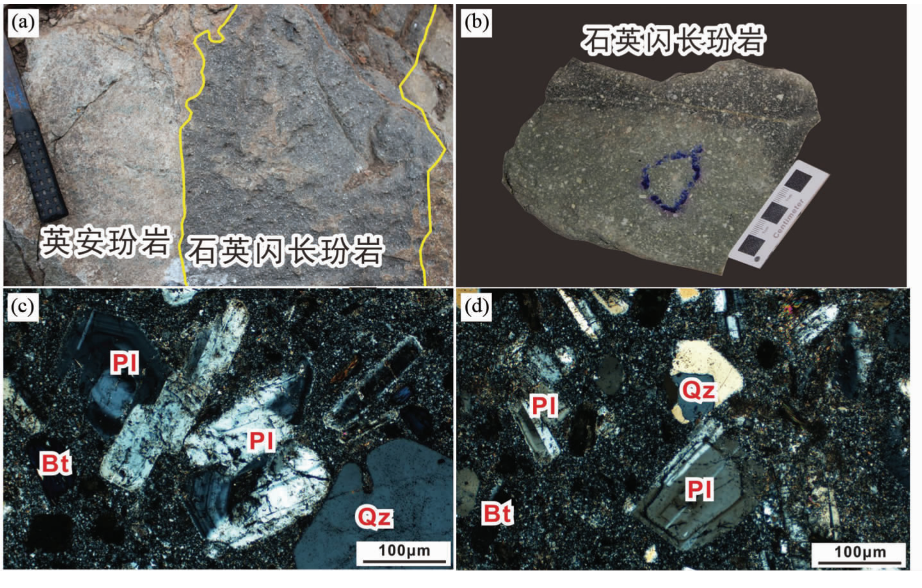

图 3 早子沟地区典型地质体接触关系和石英闪长玢岩岩相学照片

(a)石英闪长玢岩侵入英安玢岩;(b)石英闪长玢岩手标本照片;(c、d)石英闪长玢岩显微岩相学照片. Bt-黑云母;Pl-斜长石;Qz-石英

Fig. 3 Field photograph and photomicrographs of quartz diorite porphyry in the Zaozigou

(a) quartz diorite porphyry intruded dacite porphyry; (b) hand specimen photograph of quartz diorite porphyry; (c, d) photomicrographs of the quartz diorite porphyry. Bt-biotite; Pl-plagioclase; Qz-quartz

0.4g 1%浓度的 LiBr 和 0.5%浓度的 NH_4I 助溶剂。混匀后转移至 XRF 专用铂金坩埚中,在1250℃熔融,并进行 XRF 测定。全岩微量分析在河北省区域地质矿产调查研究所完成。在溶样瓶中加入 2mL 8mol/L 的 HNO_3 和 0.5mL 8mol/L 的 HF,并持续加热来溶解样品,溶解后在通风橱中蒸干样品。稍后再次加入 2mL 8mol/L 的 HNO_3 继续加热,并重复前面

表 1 早子沟石英闪长玢岩 LA-ICP-MS 锆石 U-Pb 定年结果

Table 1 LA-ICP-MS zircon U-Pb dating results of the quartz diorite porphyry in the Zaozigou

测点号	Th	U	Th/U	Isotopic ratio						Age (Ma)						谐和度
	($\times 10^{-6}$)			$^{207}Pb/^{206}Pb$	2σ	$^{207}Pb/^{235}U$	2σ	$^{206}Pb/^{238}U$	2σ	$^{207}Pb/^{206}Pb$	2σ	$^{207}Pb/^{235}U$	2σ	$^{206}Pb/^{238}U$	2σ	
样品 18ZZG16,年龄为 232.8±2.3Ma(MSWD=1.9,n=19)																
1	66	469	0.14	0.0497	0.0017	0.2498	0.0095	0.0363	0.0005	189.0	77.8	226.4	7.7	230.0	3.1	102%
2	185	993	0.19	0.0504	0.0014	0.2531	0.0084	0.0364	0.0006	213.0	64.8	229.1	6.8	230.3	3.8	101%
5	85	495	0.17	0.0512	0.0017	0.2638	0.0086	0.0376	0.0006	255.6	74.1	237.7	6.9	237.9	3.6	100%
6	212	510	0.42	0.0509	0.0017	0.2612	0.0095	0.0371	0.0005	239.0	77.8	235.6	7.7	235.1	2.9	100%
7	206	976	0.21	0.0511	0.0015	0.2555	0.0084	0.0363	0.0006	255.6	60.2	231.0	6.8	229.6	3.7	99%
10	161	641	0.25	0.0509	0.0024	0.2526	0.0123	0.0360	0.0007	239.0	109.2	228.7	10.0	228.0	4.2	100%
12	140	520	0.27	0.0509	0.0019	0.2521	0.0096	0.0360	0.0006	235.3	87.0	228.2	7.8	228.1	3.7	100%
13	202	962	0.21	0.0510	0.0014	0.2545	0.0075	0.0361	0.0005	239.0	64.8	230.2	6.1	228.6	3.1	99%
14	212	796	0.27	0.0523	0.0018	0.2677	0.0100	0.0369	0.0011	298.2	86.1	240.9	8.1	233.8	6.8	97%
17	197	931	0.21	0.0504	0.0020	0.2522	0.0100	0.0361	0.0007	213.0	92.6	228.4	8.1	228.4	4.1	100%
18	74	809	0.09	0.0507	0.0021	0.2604	0.0114	0.0369	0.0006	227.8	98.1	235.0	9.2	233.3	3.6	99%
20	62	251	0.25	0.0504	0.0026	0.2713	0.0145	0.0387	0.0005	213.0	113.9	243.7	11.6	244.8	3.3	100%
21	158	850	0.19	0.0521	0.0017	0.2697	0.0091	0.0375	0.0007	287.1	75.9	242.4	7.3	237.2	4.1	98%
22	108	350	0.31	0.0511	0.0019	0.2576	0.0104	0.0365	0.0008	255.6	80.5	232.7	8.4	230.9	4.8	99%
23	58	342	0.17	0.0514	0.0020	0.2659	0.0106	0.0375	0.0006	261.2	88.9	239.4	8.5	237.5	3.6	99%
27	148	707	0.21	0.0499	0.0022	0.2461	0.0104	0.0358	0.0004	187.1	101.8	223.4	8.5	226.8	2.6	102%
28	72	670	0.11	0.0504	0.0014	0.2580	0.0072	0.0372	0.0005	213.0	64.8	233.1	5.8	235.3	2.8	101%
29	60	431	0.14	0.0503	0.0019	0.2586	0.0107	0.0372	0.0005	209.3	89.8	233.6	8.6	235.3	3.2	101%
30	52	205	0.25	0.0505	0.0024	0.2540	0.0122	0.0366	0.0008	216.7	111.1	229.8	9.9	232.0	4.9	101%
31	130	526	0.25	0.0515	0.0024	0.2526	0.0126	0.0354	0.0006	264.9	107.4	228.7	10.2	224.5	3.7	98%
32	56	465	0.12	0.0504	0.0017	0.2556	0.0085	0.0368	0.0005	213.0	50.0	231.1	6.9	232.7	3.0	101%
35	52	421	0.12	0.0511	0.0018	0.2590	0.0094	0.0367	0.0005	242.7	81.5	233.9	7.5	232.1	3.1	99%
样品 18ZZG16,继承锆石																
15	314	454	0.69	0.1040	0.0021	1.9598	0.0439	0.1359	0.0016	1696.0	37.0	1101.8	15.1	821.2	9.0	75%
36	37	285	0.13	0.1153	0.0024	4.7739	0.1211	0.2982	0.0052	1884.9	36.7	1780.3	21.3	1682.2	25.8	94%
样品 18ZZG17,年龄为 232.1±1.4Ma(MSWD=1.9,n=25)																
2	119	899	0.13	0.0514	0.0015	0.2615	0.0086	0.0369	0.0007	257.5	68.5	235.9	6.9	233.6	4.4	99%
3	115	1071	0.11	0.0509	0.0013	0.2618	0.0081	0.0372	0.0007	239.0	52.8	236.1	6.5	235.6	4.4	100%
4	55	367	0.15	0.0515	0.0024	0.2672	0.0131	0.0376	0.0006	261.2	107.4	240.4	10.5	238.1	3.5	99%
5	194	1003	0.19	0.0504	0.0020	0.2506	0.0112	0.0359	0.0007	213.0	92.6	227.0	9.1	227.4	4.5	100%
6	40	538	0.07	0.0512	0.0018	0.2582	0.0091	0.0366	0.0006	255.6	79.6	233.2	7.4	231.8	3.7	99%
7	271	1124	0.24	0.0503	0.0013	0.2575	0.0079	0.0370	0.0007	205.6	95.4	232.6	6.3	234.4	4.1	101%
8	199	1098	0.18	0.0505	0.0014	0.2493	0.0073	0.0357	0.0007	220.4	64.8	226.0	6.0	226.0	4.1	100%
9	236	967	0.24	0.0510	0.0012	0.2586	0.0065	0.0366	0.0005	239.0	53.7	233.5	5.3	231.9	3.2	99%
10	80	1269	0.06	0.0505	0.0015	0.2495	0.0082	0.0356	0.0004	216.7	72.2	226.2	6.7	225.5	2.7	100%
12	175	1029	0.17	0.0501	0.0017	0.2517	0.0098	0.0362	0.0008	198.2	77.8	228.0	8.0	229.1	4.9	100%
13	236	1052	0.22	0.0506	0.0015	0.2515	0.0090	0.0357	0.0007	233.4	73.1	227.8	7.3	226.3	4.2	99%
16	161	760	0.21	0.0508	0.0016	0.2568	0.0080	0.0367	0.0005	231.6	67.6	232.1	6.4	232.5	3.3	100%
17	44	348	0.13	0.0497	0.0023	0.2546	0.0123	0.0371	0.0005	189.0	102.8	230.3	9.9	234.8	3.2	102%
18	190	651	0.29	0.0499	0.0012	0.2597	0.0079	0.0377	0.0006	190.8	62.0	234.4	6.4	238.3	3.7	102%
19	97	778	0.13	0.0510	0.0014	0.2575	0.0075	0.0367	0.0006	239.0	63.0	232.6	6.1	232.5	3.7	100%
20	144	814	0.18	0.0510	0.0013	0.2597	0.0074	0.0370	0.0006	242.7	54.6	234.5	6.0	234.1	4.0	100%
21	156	488	0.32	0.0503	0.0018	0.2500	0.0089	0.0361	0.0004	209.3	81.5	226.6	7.2	228.4	2.7	101%
24	93	744	0.12	0.0510	0.0016	0.2606	0.0092	0.0370	0.0007	242.7	70.4	235.1	7.4	234.3	4.5	100%
25	67	373	0.18	0.0510	0.0020	0.2524	0.0099	0.0360	0.0006	239.0	92.6	228.6	8.0	228.1	3.6	100%
29	146	724	0.20	0.0505	0.0016	0.2570	0.0089	0.0367	0.0006	216.7	72.2	232.3	7.2	232.4	3.5	100%
31	106	390	0.27	0.0523	0.0019	0.2707	0.0101	0.0373	0.0006	301.9	86.1	243.3	8.1	236.1	3.5	97%
32	62	447	0.14	0.0504	0.0017	0.2572	0.0082	0.0370	0.0005	213.0	43.5	232.4	6.6	234.0	3.1	101%
34	61	361	0.17	0.0508	0.0019	0.2613	0.0104	0.0372	0.0005	231.6	88.9	235.7	8.4	235.2	3.4	100%

续表 1

Continued Table 1

测点号	Th ($\times10^{-6}$)	U ($\times10^{-6}$)	Th/U	Isotopic ratio $^{207}Pb/^{206}Pb$	2σ	$^{207}Pb/^{235}U$	2σ	$^{206}Pb/^{238}U$	2σ	Age (Ma) $^{207}Pb/^{206}Pb$	2σ	$^{207}Pb/^{235}U$	2σ	$^{206}Pb/^{238}U$	2σ	谐和度
35	48	792	0.06	0.0510	0.0026	0.2571	0.0130	0.0364	0.0005	242.7	123.1	232.3	10.5	230.2	3.1	99%
36	53.98	193	0.28	0.0514	0.0027	0.2650	0.0138	0.0373	0.0006	261.2	88.0	238.7	11.1	236.4	3.8	99%
样品 18ZZG17，继承锆石																
14	85	427	0.20	0.1088	0.0021	4.0583	0.0957	0.2694	0.0045	1779.9	33.8	1646.0	19.3	1537.6	23.0	93%
23	48	188	0.25	0.1510	0.0027	6.8705	0.2090	0.3278	0.0073	2357.7	30.1	2094.9	27.0	1827.5	35.4	87%
27	32	282	0.11	0.1040	0.0037	2.5584	0.2993	0.1614	0.0160	1698.2	66.2	1288.8	85.4	964.6	88.6	75%
28	18	73	0.24	0.1238	0.0029	5.5034	0.1347	0.3210	0.0035	2013.0	41.8	1901.1	21.1	1794.5	17.0	94%
33	34	49	0.69	0.1043	0.0034	4.0507	0.1375	0.2802	0.0042	1702.2	59.3	1644.4	27.7	1592.4	21.3	97%

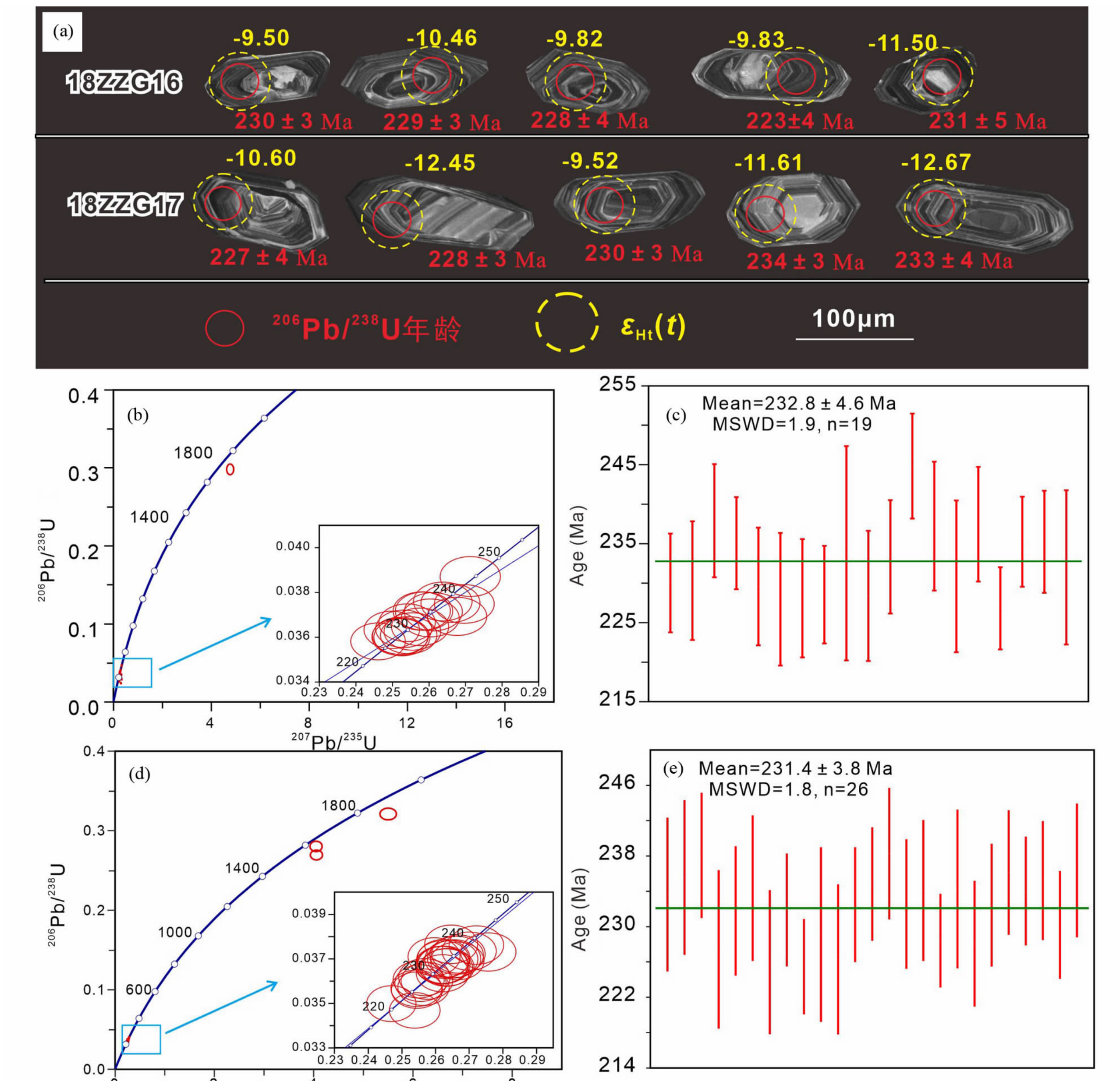

图 4 早子沟石英闪长玢岩典型锆石阴极发光图像(a)和锆石 LA-ICP-MS U-Pb 年龄谐和图(b-e)

Fig. 4 Representative zircon cathodoluminescence images (a) and zircon LA-ICP-MS U-Pb concordia diagrams (b-e) of the quartz diorite porphyry in the Zaozigou

表2 早子沟石英闪长玢岩主量元素(wt%)与微量元素($\times10^{-6}$)分析结果

Table 2 Major (wt%) and trace ($\times10^{-6}$) element compositions of the quartz diorite porphyry in the Zaozigou

样品号	18ZZG16	18ZZG17	18ZZG18	18ZZG19	18ZZG20	18ZZG21	18ZZG22	18ZZG23
SiO_2	59.69	62.27	59.67	56.18	68.26	60.16	64.12	62.13
Al_2O_3	16.85	16.57	18.00	16.50	16.40	16.70	18.00	17.70
TiO_2	0.64	0.63	0.71	0.61	0.34	0.56	0.69	0.57
Fe_2O_3	1.36	1.54	1.31	2.15	0.63	0.82	0.90	1.10
FeO	4.18	3.35	3.95	3.68	2.08	3.98	3.65	3.16
$Fe_2O_3{}^T$	5.40	4.74	5.59	6.24	3.13	5.35	5.25	4.96
MnO	0.10	0.06	0.08	0.11	0.05	0.08	0.07	0.07
MgO	4.13	2.41	4.10	6.27	2.45	6.28	2.30	3.65
CaO	6.32	4.87	5.72	6.91	4.19	5.80	5.42	5.68
Na_2O	2.16	2.35	2.86	4.02	3.36	3.20	3.23	3.34
K_2O	1.82	2.51	1.95	3.19	3.70	2.23	3.34	3.02
P_2O_5	0.11	0.10	0.12	0.19	0.09	0.11	0.19	0.11
LOI	2.49	3.19	2.57	2.02	0.92	2.54	1.03	2.23
Total	99.84	99.84	99.86	99.69	99.88	99.85	99.80	99.86
$Mg^{\#}$	57.67	47.57	58.76	66.56	62.26	70.35	47.90	61.06
Na_2O+K_2O	3.98	4.86	4.81	7.21	7.06	5.43	6.57	6.36
K_2O/Na_2O	0.84	1.07	0.68	0.79	1.10	0.70	1.03	0.90
A/CNK	0.99	1.07	1.04	0.73	0.95	0.92	0.96	0.93
A/NK	3.05	2.51	2.64	1.64	1.72	2.17	2.01	2.02
Sc	9.24	4.99	16.00	21.50	9.20	16.00	9.90	12.60
V	30.03	12.43	84.00	157.0	51.00	106.0	56.00	84.00
Co	6.75	3.75	17.10	22.80	9.30	24.70	10.40	12.20
Ni	3.64	3.87	27.70	51.00	19.70	82.80	5.00	21.10
Cu	8.07	11.15	35.00	45.00	186.0	4.00	3.00	13.00
Ga	10.67	11.17	19.70	18.80	16.40	16.90	21.80	17.50
Sr	179.0	162.3	333.0	1304	314.0	411.0	578.0	385.0
Y	8.70	4.26	20.95	21.44	18.09	17.60	20.34	20.17
Zn	18.71	23.67	73.00	66.00	35.00	44.00	63.00	43.00
Nb	4.20	4.92	11.40	8.20	9.70	9.80	14.90	11.00
Ba	351.7	348.0	567.0	1169	481.0	422.0	1111	560.0
Mo	0.09	0.14	0.42	0.33	0.30	0.13	0.16	0.17
Cs	5.96	4.10	11.17	7.57	18.70	24.88	6.06	4.24
Ta	0.38	0.41	0.79	0.67	1.03	0.87	1.03	0.80
W	0.37	0.58	1.36	2.19	3.30	1.37	0.89	0.78
Pb	3.73	9.54	24.20	37.10	28.90	8.60	32.30	16.20
Bi	0.09	0.04	0.06	0.43	2.77	0.62	0.11	0.24
Th	5.22	7.72	8.30	9.20	19.10	10.80	14.90	12.40
U	1.83	1.70	2.40	4.30	2.70	3.10	4.60	1.50
Sc	9.24	4.99	16.52	22.02	9.29	16.97	10.42	14.62
Be	1.40	1.63	2.51	2.33	3.48	2.75	3.96	2.89
Cr	13.58	8.22	126.0	149.0	90.00	350.0	32.00	147.0
Li	22.77	19.78	39.00	98.00	41.00	89.00	71.00	54.00
La	16.48	21.67	28.12	38.43	31.39	22.70	52.86	34.97
Ce	32.09	42.91	58.45	81.42	63.80	47.68	106.8	72.09
Pr	3.79	4.82	6.84	10.10	6.93	5.35	12.15	8.05
Nd	14.16	17.48	25.67	38.37	24.15	19.90	43.65	28.71
Sm	2.73	2.93	5.09	6.31	4.57	3.92	7.72	5.28
Eu	0.69	0.64	1.25	1.76	0.87	1.01	1.76	1.07
Gd	2.43	2.32	4.74	4.92	3.82	3.57	6.07	4.51
Tb	0.36	0.28	0.76	0.71	0.61	0.57	0.83	0.71
Dy	1.85	1.09	4.19	3.95	3.39	3.29	4.30	3.95
Ho	0.33	0.16	0.79	0.79	0.66	0.65	0.77	0.77
Er	0.87	0.39	2.17	2.30	1.93	1.89	2.02	2.13

续表 2

Continued Table 2

样品号	18ZZG16	18ZZG17	18ZZG18	18ZZG19	18ZZG20	18ZZG21	18ZZG22	18ZZG23
Tm	0. 12	0. 05	0. 34	0. 37	0. 31	0. 31	0. 31	0. 34
Yb	0. 72	0. 25	2. 11	2. 42	2. 08	2. 01	1. 95	2. 24
Lu	0. 11	0. 04	0. 32	0. 39	0. 33	0. 32	0. 29	0. 33
∑REE	76. 74	95. 02	140. 8	192. 2	144. 8	113. 2	241. 5	165. 2
LREE	69. 94	90. 45	125. 4	176. 4	131. 7	100. 6	224. 9	150. 2
HREE	6. 80	4. 57	15. 42	15. 85	13. 13	12. 61	16. 54	14. 98
LREE/HREE	10. 29	19. 80	8. 13	11. 13	10. 03	7. 97	13. 60	10. 02
$(La/Yb)_N$	16. 40	61. 20	9. 56	11. 39	10. 83	8. 10	19. 44	11. 20
δEu	0. 80	0. 73	0. 77	0. 93	0. 62	0. 81	0. 76	0. 65

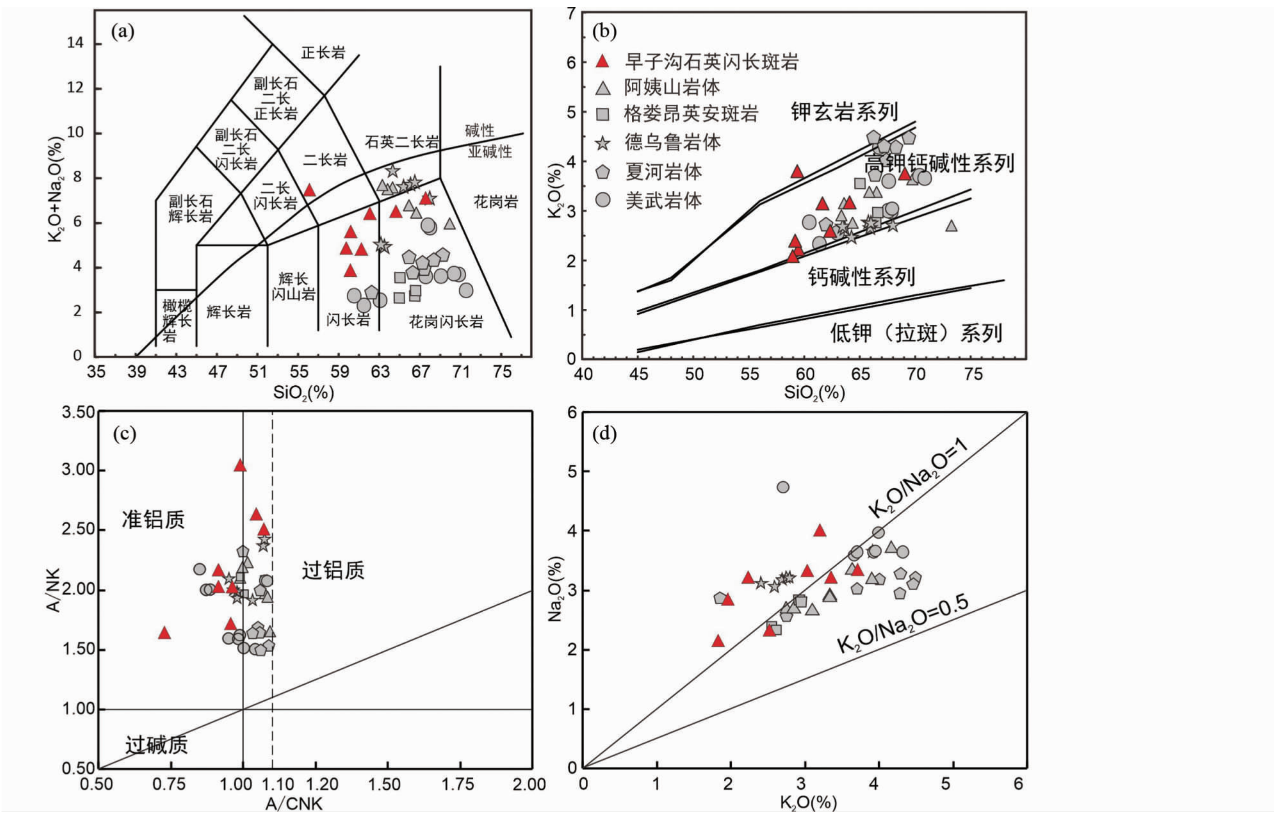

图 5　早子沟石英闪长玢岩地球化学图解

(a) TAS 图解(Chappell and White, 1974);(b) K_2O-SiO_2 图解(Middlemost, 1994);(c) A/NK-A/CNK 图解, A/CNK = Al_2O_3/($CaO + Na_2O + K_2O$), A/NK = Al_2O_3/($Na_2O + K_2O$)(Frost *et al.*, 2001);(d) Na_2O-K_2O 图解．数据来源:骆必继,2013;韦萍等,2013;徐学义等,2014; Qiu and Deng, 2017;黄雅琪等,2020;图 6、图 8-图 10 的数据来源及图例同此图

Fig. 5　Geochemical plots for rocks of quartz diorite porphyry in the Zaozigou

(a) Total alkali silica (Chappell and White, 1974); (b) K_2O vs. SiO_2 (Middlemost, 1994); (c) A/NK vs. A/CNK, A/CNK = Al_2O_3/($CaO + Na_2O + K_2O$) (Frost *et al.*, 2001); (d) Na_2O vs. K_2O. Data from Luo, 2013; Wei *et al.*, 2013; Xu *et al.*, 2014; Qiu and Deng, 2017; Huang *et al.*, 2020. Data sources and legends in Fig. 6 and Fig. 8-Fig. 10 are same as in this figure

工作。最后用 8mol/L 的 HNO_3 溶解样品,之后加去离子水稀释至 250mL,取出部分进行 ICP-MS 分析。

4　分析结果

4.1　锆石 U-Pb 年代学

对 2 件石英闪长玢岩样品(18ZZG16 和 18ZZG17)进行

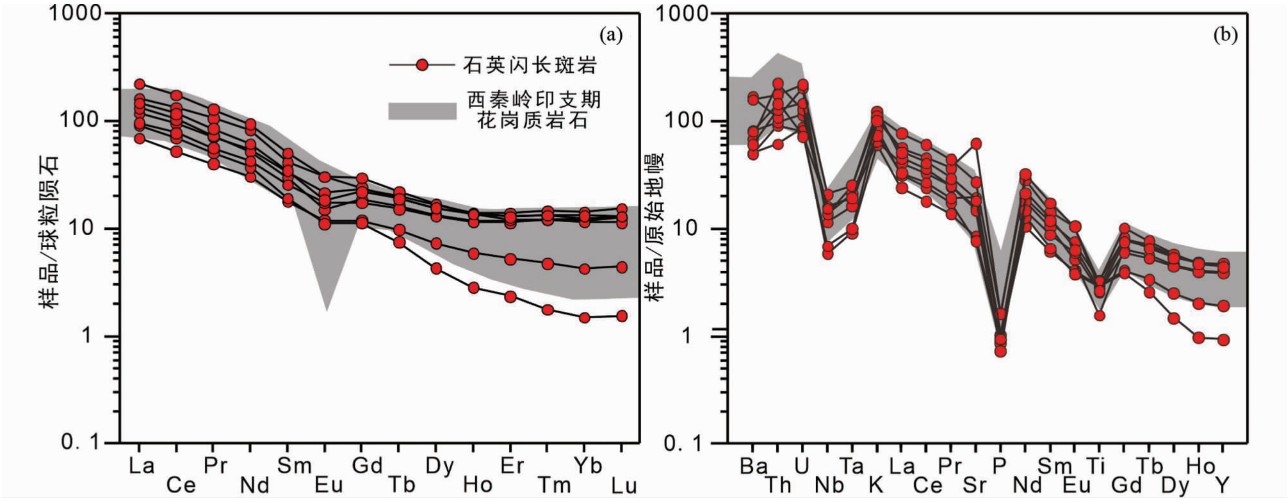

图6 早子沟石英闪长玢岩球粒陨石标准化稀土元素配分模式图(a,标准化值据 Boynton, 1984)与原始地幔标准化微量元素蛛网图(b,标准化值据 Sun and McDonough, 1989)

Fig. 6 Chondrite-normalized REE patterns (a, normalization values after Boynton, 1984) and primitive mantle-normalized trace element spider diagrams (b, normalization values after Sun and McDonough, 1989) of quartz diorite porphyry in the Zaozigou

锆石 LA-ICP-MS U-Pb 定年,测年结果如表 1 所示。通过阴极发光图像(图 4a)可以看出,石英闪长玢岩中多数锆石颗粒是自形的,并显示出良好的振荡生长环带。这些锆石长度多在 100~200μm,长宽比为 2:1 到 3:1,呈长柱状,Th/U 多大于 0.2,符合岩浆锆石特征(Fu *et al.*, 2021; Wu *et al.*, 2022)。每个样品选取 36 颗锆石进行测试,18ZZG16 样品有 2 个继承锆石,除继承锆石外加权平均 $^{206}Pb/^{238}U$ 年龄为 232.8±4.6Ma(MSWD=1.9,n=19;图 4b, c);18ZZG17 样品有 5 个继承锆石,除继承锆石外加权平均 $^{206}Pb/^{238}U$ 年龄为 231.4±3.8Ma(MSWD=1.8,n=26;图 4d, e)。

4.2 岩石地球化学特征

8 件石英闪长玢岩样品主量和微量元素地球化学分析结果如表 2 所示。石英闪长玢岩 SiO_2 含量为 56.18%~68.26%,Al_2O_3 含量为 16.40%~18.00%,TiO_2 含量为 0.34%~0.71%,MgO 含量为 2.30%~6.28%,K_2O 含量为 1.82%~3.70%,Na_2O 含量为 2.16%~4.02%,K_2O/Na_2O 值为 0.68~1.10(图 5),$Mg^{\#}$ 为 47.57~70.35,具有高 Al 中 Mg 的特点。在 TAS 判别图解中,样品落在闪长岩-花岗闪长岩区域内(图 5a),其 A/CNK 为 0.73~1.07,A/NK 为 1.64~3.05,属于准铝质-弱过铝质系列岩石。在 SiO_2-K_2O 图解中,显示出钙碱性-高钾钙碱性特征(图 5b, c)。稀土元素总量(∑REE)为 76.74×10^{-6}~241.5×10^{-6},LREE/HREE 为 7.97~19.8,$(La/Yb)_N$ 比值为 8.10~61.2,轻重稀土分异较大,稀土配分曲线为轻稀土富集、重稀土平坦的右倾型(图 6a),具有弱负铕异常(δEu=0.65~0.93)。微量元素蛛网图显示,岩石含有少量 Ni(3.64×10^{-6}~82.80×10^{-6})和 Co(3.75×10^{-6}~24.70×10^{-6}),并且富集大离子亲石元素(K、Sr、Ba、Cs),亏损 Sr 和高场强元素 Nb、Ta 等(图 6b)。

4.3 锆石 Lu-Hf 同位素

石英闪长玢岩(18ZZG16、18ZZG17)锆石 Lu-Hf 同位素分析结果如表 3 和图 7 所示。假设大陆地壳的平均 $^{176}Lu/^{177}Hf$ 值为 0.015 来计算岩浆岩的二阶段模型年龄(t_{DM}^2)(Griffin *et al.*, 2002; Qiu *et al.*, 2016a, 2017)。2 件石英闪长玢岩 48 个测点的 $^{176}Hf/^{177}Hf$ 值为 0.282266~0.282434,$^{176}Lu/^{177}Hf$ 值为 0.0000~0.0010,均小于 0.002。$\varepsilon_{Hf}(t)$ 值在 -12.9~-7.2,对应二阶段模式年龄 t_{DM}^2 在 1.70~2.10Ga(图 7)。样品的 $^{176}Lu/^{177}Hf$ 值均小于 0.002,表明 $^{176}Lu/^{177}Hf$ 能较好反应其形成过程 Hf 同位素组成(Zheng *et al.*, 2006; 吴福元等, 2007)。

5 讨论

5.1 早-中三叠世岩浆活动

早子沟地区主要发育花岗闪长玢岩、英安玢岩和石英闪长玢岩等火成岩,岩性呈现由中酸性向中性过渡。石英闪长玢岩侵入英安玢岩中,暗示石英闪长玢岩侵位时间晚于英安玢岩(图 3a)。中酸性岩脉(花岗闪长玢岩脉和英安玢岩)锆石年龄多在 250~236Ma;中性岩脉如石英闪长斑(玢)岩等显示的年龄范围约为 236~233Ma(隋吉祥和李建威, 2013; 第鹏飞, 2018; 耿建珍等, 2019; Yu *et al.*, 2019)。本文研究的石英闪长玢岩锆石 U-Pb 年龄为 ~232Ma,是该地区中三叠世岩浆活动的产物。结合前人对早子沟地区赋矿围岩岩相学和年代学的研究,可以发现该区早-中三叠世岩浆侵位时间约为 250~232Ma,按侵位时间和岩性大致可分为两

表 3　早子沟石英闪长玢岩 LA-MC-ICP-MS 锆石 Lu-Hf 同位素分析结果

Table 3　LA-MC-ICP-MS zircon Lu-Hf isotope composition of the quartz diorite porphyry in the Zaozigou

测点号	Age (Ma)	$^{176}Lu/^{177}Hf$	2σ	$^{176}Hf/^{177}Hf$	2σ	$\varepsilon_{Hf}(0)$	$\varepsilon_{Hf}(t)$	t^1_{DM}(Ma)	t^2_{DM}(Ma)	$f_{Lu/Hf}$
样品 18ZZG16										
1	230	0.0000	0.0000	0.282278	0.000017	-17.5	-12.4	1339	2041	-1.00
2	230	0.0006	0.0000	0.282315	0.000015	-16.2	-11.2	1309	1964	-0.98
5	238	0.0008	0.0000	0.282348	0.000015	-15.0	-9.9	1270	1889	-0.98
6	235	0.0003	0.0000	0.282332	0.000015	-15.6	-10.5	1276	1922	-0.99
7	230	0.0005	0.0000	0.282329	0.000019	-15.7	-10.7	1286	1932	-0.98
10	228	0.0007	0.0000	0.282403	0.000017	-13.1	-8.2	1189	1772	-0.98
12	228	0.0001	0.0000	0.282274	0.000019	-17.6	-12.6	1346	2053	-1.00
13	229	0.0006	0.0000	0.282364	0.000015	-14.4	-9.5	1240	1857	-0.98
14	234	0.0008	0.0000	0.282411	0.000018	-12.8	-7.8	1183	1751	-0.98
17	228	0.0005	0.0000	0.282370	0.000015	-14.2	-9.3	1231	1843	-0.98
18	233	0.0001	0.0000	0.282336	0.000016	-15.4	-10.3	1263	1912	-1.00
20	245	0.0001	0.0000	0.282340	0.000019	-15.3	-9.9	1259	1896	-1.00
21	237	0.0007	0.0000	0.282384	0.000017	-13.7	-8.6	1216	1808	-0.98
22	231	0.0000	0.0000	0.282339	0.000017	-15.3	-10.2	1257	1905	-1.00
23	237	0.0002	0.0000	0.282329	0.000016	-15.7	-10.5	1277	1926	-0.99
27	227	0.0000	0.0000	0.282357	0.000019	-14.7	-9.7	1232	1867	-1.00
28	235	0.0001	0.0000	0.282297	0.000019	-16.8	-11.7	1317	1998	-1.00
29	235	0.0000	0.0000	0.282353	0.000018	-14.8	-9.7	1238	1872	-1.00
30	232	0.0000	0.0000	0.282293	0.000017	-17.0	-11.9	1319	2008	-1.00
31	225	0.0002	0.0000	0.282332	0.000015	-15.6	-10.7	1273	1927	-0.99
32	233	0.0001	0.0000	0.282328	0.000018	-15.7	-10.6	1273	1930	-1.00
35	232	0.0002	0.0000	0.282316	0.000016	-16.1	-11.1	1294	1958	-0.99
样品 18ZZG16,继承锆石										
15	821	0.0005	0.0000	0.281567	0.000018	-42.6	-24.8	2329	3251	-0.98
36	1682	0.0003	0.0000	0.281602	0.000013	-41.4	-4.3	2269	2633	-0.99
样品 18ZZG17										
2	234	0.0001	0.0000	0.282269	0.000019	-17.8	-12.7	1353	2060	-1.00
3	236	0.0002	0.0000	0.282298	0.000019	-16.8	-11.6	1317	1995	-1.00
4	238	0.0001	0.0000	0.282299	0.000015	-16.7	-11.5	1312	1990	-1.00
5	227	0.0009	0.0000	0.282357	0.000018	-14.7	-9.8	1260	1877	-0.97
6	232	0.0000	0.0000	0.282350	0.000017	-14.9	-9.8	1241	1880	-1.00
7	234	0.0005	0.0000	0.282342	0.000019	-15.2	-10.2	1268	1902	-0.99
8	226	0.0006	0.0000	0.282342	0.000018	-15.2	-10.4	1273	1908	-0.98
9	232	0.0008	0.0000	0.282371	0.000017	-14.2	-9.2	1239	1842	-0.98
10	225	0.0002	0.0000	0.282285	0.000018	-17.2	-12.3	1336	2031	-1.00
12	229	0.0003	0.0000	0.282307	0.000019	-16.5	-11.5	1310	1981	-0.99
13	226	0.0007	0.0000	0.282352	0.000019	-14.9	-10.0	1260	1885	-0.98
16	232	0.0005	0.0000	0.282329	0.000015	-15.7	-10.7	1287	1932	-0.98
17	235	0.0000	0.0000	0.282274	0.000018	-17.6	-12.5	1345	2048	-1.00
18	238	0.0002	0.0000	0.282318	0.000015	-16.1	-10.9	1290	1950	-0.99
20	234	0.0006	0.0000	0.282390	0.000017	-13.5	-8.5	1206	1795	-0.98
21	228	0.0001	0.0000	0.282319	0.000016	-16.0	-11.0	1287	1953	-1.00
22	273	0.0004	0.0000	0.281988	0.000017	-27.7	-21.8	1748	2659	-0.99
24	234	0.0003	0.0000	0.282359	0.000016	-14.6	-9.5	1237	1862	-0.99
25	228	0.0000	0.0000	0.282383	0.000018	-13.7	-8.7	1196	1808	-1.00
29	232	0.0006	0.0000	0.282331	0.000018	-15.6	-10.6	1286	1928	-0.98
31	236	0.0003	0.0000	0.282347	0.000017	-15.0	-9.9	1254	1887	-0.99
32	234	0.0000	0.0000	0.282319	0.000017	-16.0	-10.9	1284	1949	-1.00
34	235	0.0001	0.0000	0.282325	0.000014	-15.8	-10.7	1279	1935	-1.00
35	230	0.0001	0.0000	0.282271	0.000018	-17.7	-12.7	1351	2057	-1.00
36	236	0.0004	0.0000	0.282325	0.000014	-15.8	-10.7	1287	1936	-0.99

续表 3

Continued Table 3

测点号	Age (Ma)	$^{176}Lu/^{177}Hf$	2σ	$^{176}Hf/^{177}Hf$	2σ	$\varepsilon_{Hf}(0)$	$\varepsilon_{Hf}(t)$	t_{DM}^{1}(Ma)	t_{DM}^{2}(Ma)	$f_{Lu/Hf}$
样品 18ZZG17,继承锆石										
14	1538	0.0012	0.0000	0.281584	0.000022	-42.0	-9.0	2343	2815	-0.97
23	1828	0.0006	0.0000	0.281795	0.000028	-34.6	5.5	2023	2142	-0.98
28	1794	0.0000	0.0000	0.281605	0.000017	-41.3	-1.3	2249	2536	-1.00
30	221	0.0003	0.0000	0.282343	0.000018	-15.2	-10.4	1258	1904	-0.99
33	1592	0.0007	0.0000	0.281536	0.000021	-43.7	-9.1	2384	2862	-0.98

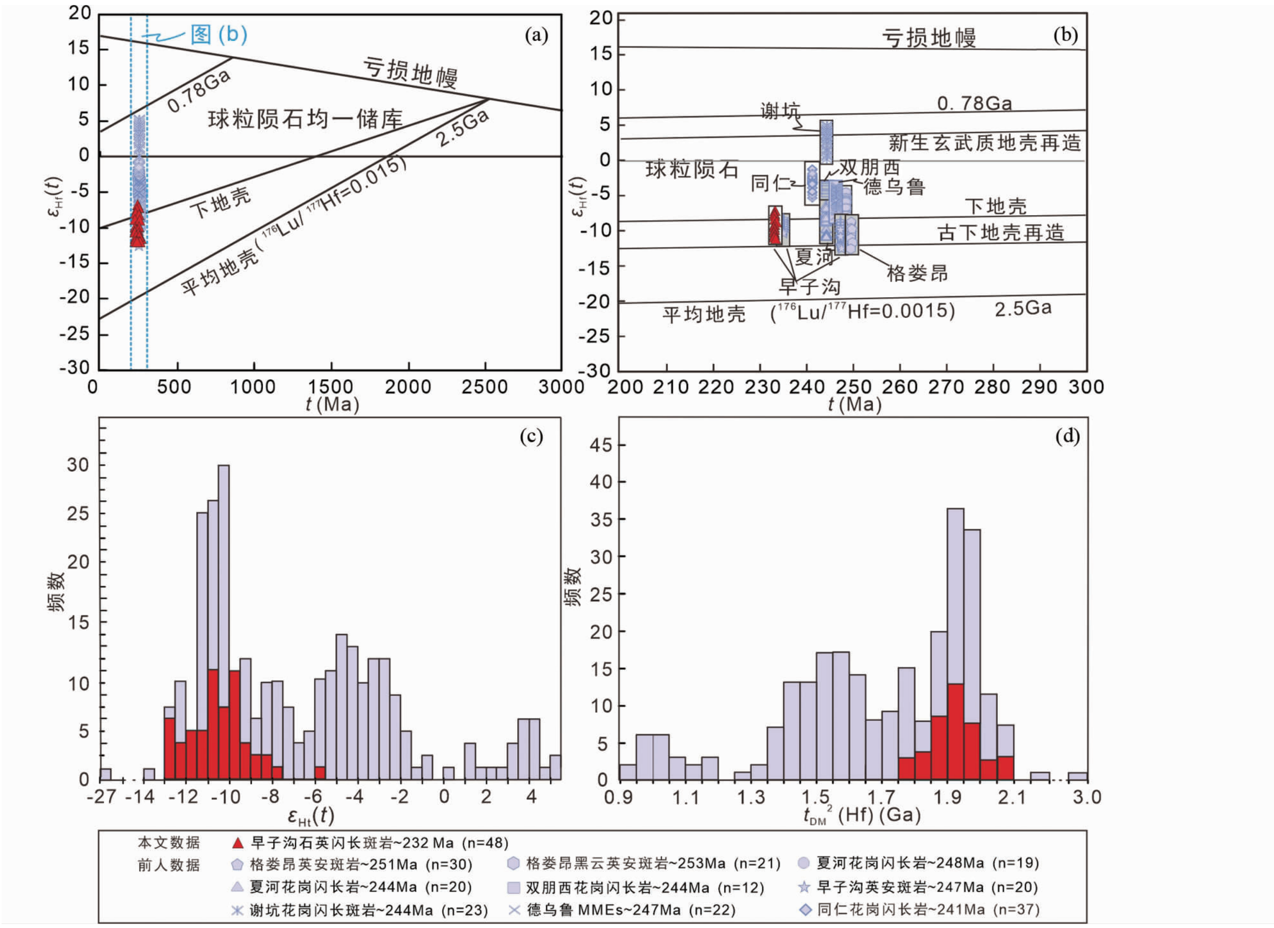

图 7 夏河-合作地区三叠纪花岗质岩石锆石 $\varepsilon_{Hf}(t)$-t 图解(a、b)、$\varepsilon_{Hf}(t)$频率直方图(c)和 t_{DM}^{2} 频率直方图(d)

数据来源:Luo *et al.*, 2012;韦萍等,2013;Li *et al.*, 2015a;Qiu and Deng, 2017;Yu *et al.*, 2019;耿建珍等,2019;黄雅琪等,2020

Fig. 7 Variations of $\varepsilon_{Hf}(t)$ vs. Age (a, b), histograms of $\varepsilon_{Hf}(t)$ (c) and histograms of corresponding two-stage Hf model ages (t_{DM}^{2}) (d) of zircons of the Triassic granitoids in the Xiahe-Hezuo district

Data from Luo *et al.*, 2012; Wei *et al.*, 2013; Li *et al.*, 2015a; Qiu and Deng, 2017; Yu *et al.*, 2019; Geng *et al.*, 2019; Huang *et al.*, 2020

类:英安玢岩和花岗闪长玢岩的侵位主要集中在 250 ~ 236Ma,而石英闪长玢岩侵位于 236 ~ 232Ma。

研究表明,西秦岭三叠纪岩浆爆发事件可分为两期,包括早-中三叠世(250 ~ 235Ma)和晚三叠世(225 ~ 205Ma)(金维浚等, 2005; Zhang *et al.*, 2007; Li *et al.*, 2014; Luo *et al.*, 2012, 2015; Zhu *et al.*, 2013)。夏河-合作地区仅存在 250 ~ 235Ma 的岩浆活动。阿夷山岩浆侵位时间为 242 ~ 238Ma,德武鲁杂岩体岩浆侵位时间为 247 ~ 238Ma,铜仁岩体岩浆侵位时间为 242 ~ 238Ma,美武岩体岩浆侵位时间为 251 ~ 243Ma,均与早-中三叠世(250 ~ 235Ma)的岩浆侵位时间一致(徐学义等, 2014; Li *et al.*, 2015b; Qiu and Deng, 2017)。与夏河-合作地区火成岩体侵位时间相似,本文早子沟石英闪长玢岩锆石 U-Pb 年龄在 ~232Ma,表明第一期(250 ~ 235Ma)岩浆活动很有可能持续到 232Ma 左右,才进

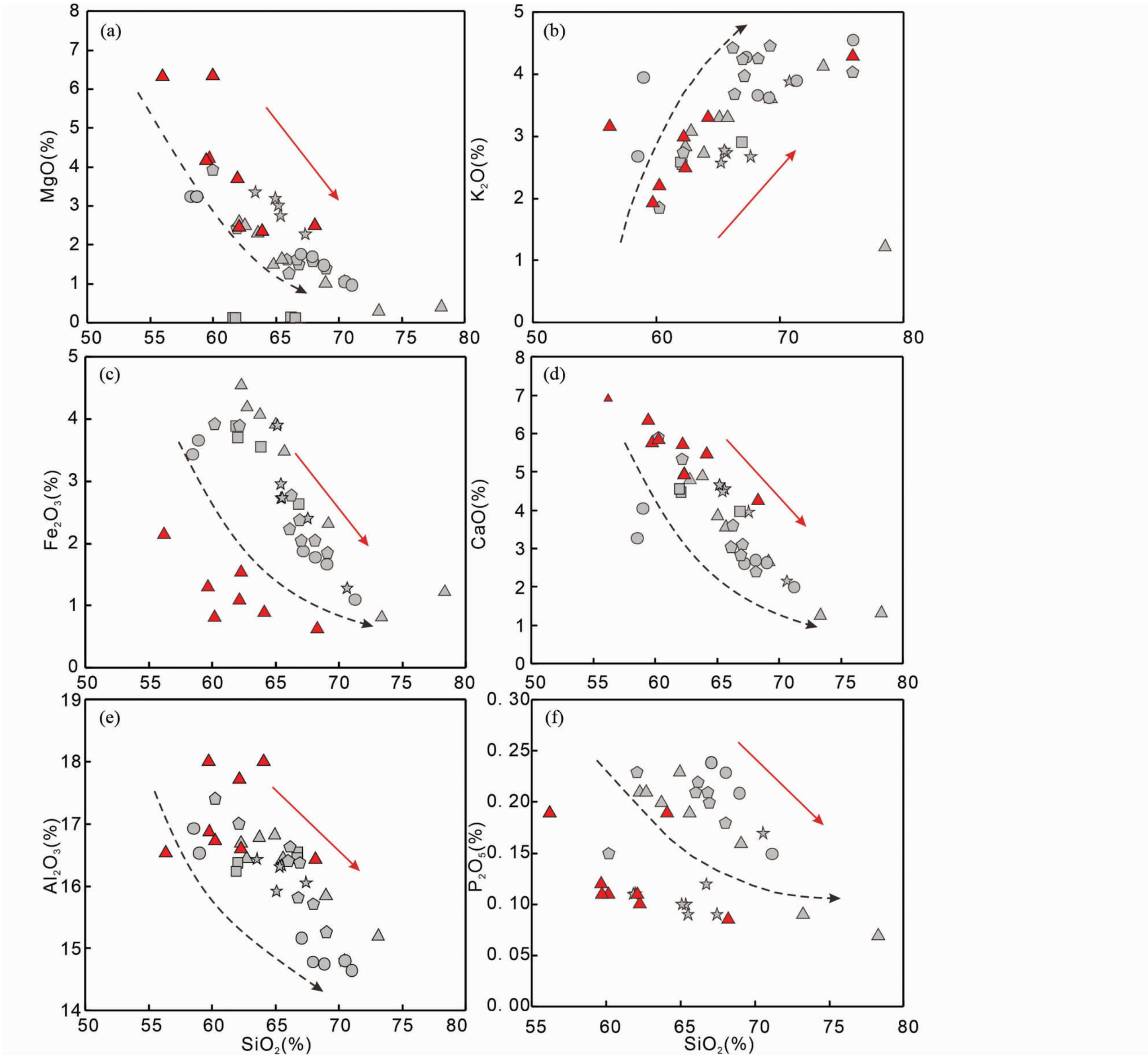

图 8 早子沟石英闪长玢岩哈克图解

Fig. 8 Harker diagrams for the quartz diorite porphyry in the Zaozigou

入到岩浆间歇期。

5.2 岩石成因与岩浆源区

在哈克图解(图 8)中,石英闪长玢岩 MgO、Fe_2O_3、CaO、Al_2O_3 和 P_2O_5 含量与 SiO_2 呈负相关,可能是角闪石、黑云母及副矿物磷灰石的分离结晶导致的(Zou *et al.*, 2022)。SiO_2 与 K_2O 呈正相关(图 8b),表明源区不存在钾长石的分离结晶。微量元素特征富含 LREE,亏损 HREE,尤其是 Ba、Nb 含量显著减少(图 6),显示了典型的大陆地壳岩石特征;较弱的负 Eu 异常(0.62 ~ 0.93)显示源区中存在斜长石或斜长石发生了分离结晶;相对平坦的 HREE 模式(图 6a)暗示源区几乎没有石榴石残留(Moyen, 2009)。石英闪长玢岩亏损高场强元素(Nb、Ta),富集大离子亲石元素,这些地球化学特征可能是下地壳部分熔融的结果(Chappell, 1999; Clemens *et al.*, 2011)。此外,石英闪长玢岩 Sr(162.3×10^{-6} ~ 1304×10^{-6})和 Nd(14.16×10^{-6} ~ 43.65×10^{-6})含量相对较高,这些元素是直接继承于岩浆源,即岩石具有深部下地壳来源,浅部的地壳过程(如分离结晶和上地壳混染)不能导致的高 Sr 和 Nd 含量(Roden and Shimizu, 2000)。La/Yb-La 和 CaO/Al_2O_3-MgO 图解表明岩浆演化主要受岩石部分熔融影响,同时矿物的分离结晶也起到部分作用(图 9a, b)。

与夏河-合作地区其他火成岩体特征一致,早子沟石英闪长玢岩也显示为准铝质-弱过铝质性质(A/CNK < 1.1)(图 5b),具有中等的 SiO_2(56.18% ~ 68.26%)、MgO(2.30% ~ 6.27%),较高的 K_2O(1.82% ~ 3.70%)(图 5d),

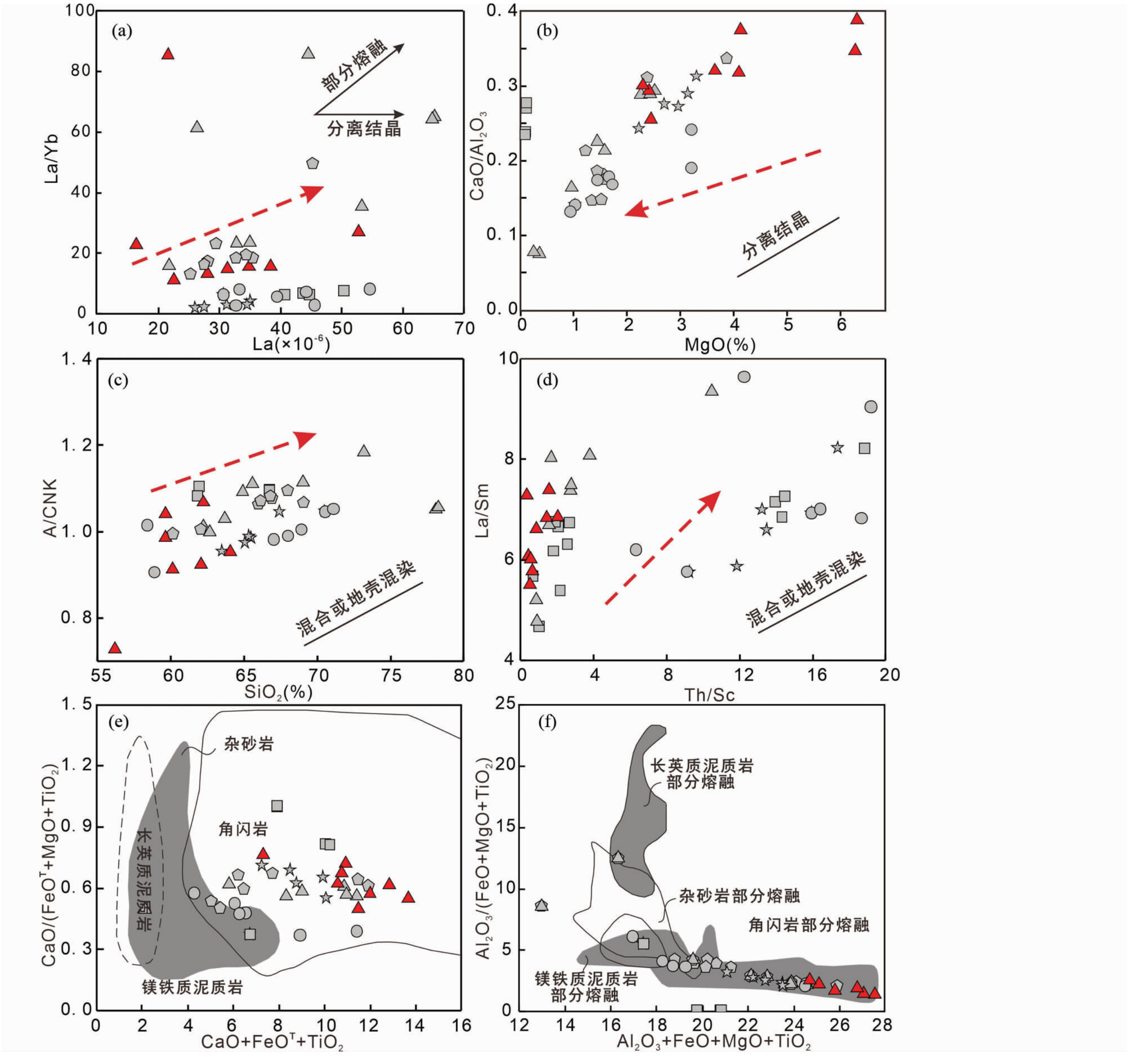

图 9 早子沟石英闪长玢岩岩石成因图解

(a) La-La/Yb 图解; (b) MgO-CaO/Al_2O_3 图解; (c) SiO_2-A/CNK 图解(Allègre and Minster, 1978); (d) Th/Sc-La/Sm 图解(Allègre and Minster, 1978); (e) $CaO/(FeO^T+MgO+TiO_2)$-$(CaO+FeO^T+TiO_2)$(Douce, 1999); (f) $Al_2O_3/(FeO+MgO+TiO_2)$-$(Al_2O_3+FeO+MgO+TiO_2)$图解(Douce, 1999), $FeO=0.8998\times Fe_2O_3{}^T$

Fig. 9 Petrogenetic discrimination diagrams for quartz diorite porphyry in the Zaozigou

(a) plot of La vs. La/Yb; (b) plot of MgO vs. CaO/Al_2O_3; (c) plot of SiO_2 vs. A/CNK (Allègre and Minster, 1978); (d) plot of Th/Sc vs. La/Sm (Allègre and Minster, 1978); (e) $CaO/(FeO^T+MgO+TiO_2)$ vs. $CaO+FeO^T+TiO_2$ diagram (Douce, 1999); (f) plot of $Al_2O_3/(FeO+MgO+TiO_2)$ vs. $Al_2O_3+FeO+MgO+TiO_2$ (Douce, 1999), $FeO=0.8998\times Fe_2O_3{}^T$

明显缺乏典型的碱性镁铁质矿物和过铝质矿物,具有与I型花岗岩类似性质。虽然具有较高的Sr($162.3\times10^{-6}\sim1304\times10^{-6}$)和较低的Y($4.26\times10^{-6}\sim21.44\times10^{-6}$),但Sr/Y值并不能作为判别是否为埃达克质岩的依据,且其$(La/Yb)_N$比值较低,多在8.10~19.44,与埃达克岩的性质不同。对于I型花岗岩岩浆源区主要存在两种认识:一种是幔源镁铁质岩浆通过岩浆混合与地壳岩浆相互作用(Kemp *et al.*, 2007);另一种是由地幔衍生熔体分离结晶产生的,但通常具有较高的SiO_2浓度(>70%)和较高A/CNK比值(1.03~2.07)(Skjerlie and Johnston, 1993; Soesoo, 2000)。本文多种证据表明石英闪长玢岩源区与第一种机制相似。石英闪长玢岩地球化学特征显示为钙碱性-高钾钙碱性特征(图

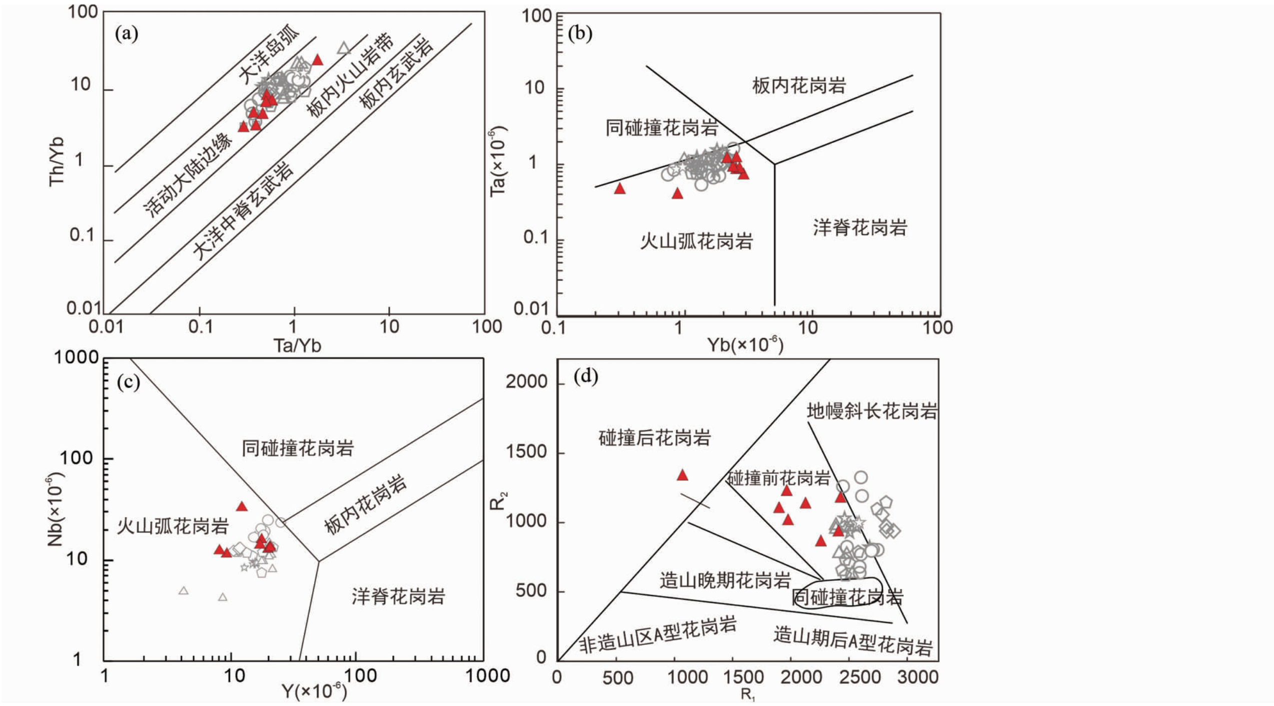

图 10　早子沟石英闪长玢岩构造图解

(a) Th/Yb-Ta/Yb 图解(Gorton and Schandl, 2000);(b) Ta-Yb 图解(Pearce *et al.*, 1984);(c) Nb-Y 图解(Pearce *et al.*, 1984);(d) R_2-R_1 图解(Batchelor and Bowden, 1985)

Fig. 10　Tectonic discrimination diagrams of the quartz diorite porphyry in the Zaozigou

(a) Th/Yb vs. Ta/Yb diagram (after Gorton and Schandl, 2000); (b) Ta vs. Yb diagram (after Pearce *et al.*, 1984); (c) Nb vs. Y diagram (after Pearce *et al.*, 1984); (d) R_2-R_1 diagram (after Batchelor and Bowden, 1985)

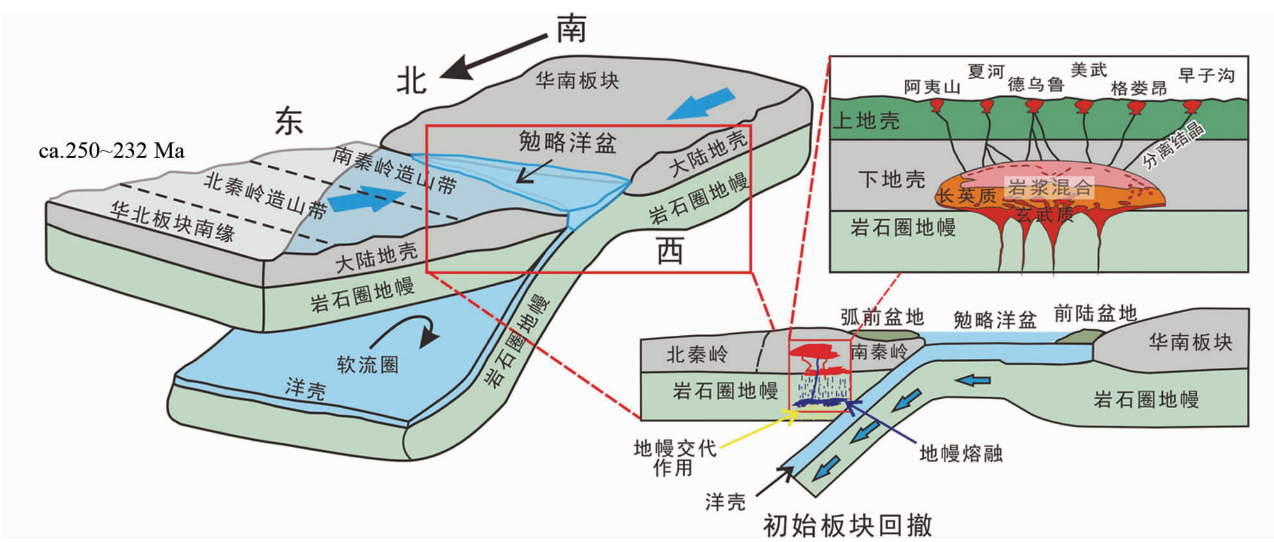

图 11　早子沟地区早-中三叠世岩浆岩成因模式图(据 Qiu and Deng, 2017;He *et al.*, 2021)

Fig. 11　Genetic model showing Early-Middle Triassic magmatic rocks in the Zaozigou (after Qiu and Deng, 2017; He *et al.*, 2021)

5c),含有较高的 K,其 K_2O 的富集主要来自岩浆源区,与中高钾镁铁质下地壳部分熔融产生的成分一致(Sisson *et al.*, 2005; Miller *et al.*, 1999)。通常,玄武质下地壳岩浆分馏很难生成 $Mg^{\#}$ 值高于 45 的中性岩石,且 $K_2O/Na_2O<1$(Rapp and Watson, 1995; Blatter *et al.*, 2013; Nandedkar *et al.*, 2014),但玄武岩岩浆和长英质熔体之间的混合可以产生

$Mg^{\#}$明显较高(>50)的中性岩石。夏河-合作地区各类岩体$Mg^{\#}$值在47.57~70.35之间,K_2O/Na_2O在0.84~1.10(图5d),表明其不能仅通过基性下地壳的部分熔融产生,幔源岩浆也起到重要作用。A/CNK-SiO_2和La/Sm-Th/Sc图解(图9c, d)均显示一定的正相关关系,也支持幔源物质参与这一观点。在$CaO/(FeO^T+MgO+TiO_2)$-$(CaO+FeO^T+TiO_2)$和$Al_2O_3/(FeO+MgO+TiO_2)$-$(Al_2O_3+FeO+MgO+TiO_2)$图解中,石英闪长玢岩均落在角闪岩的部分熔融区域内,进一步表明其主要来源于富钾玄武质变火成岩的部分熔融,与西秦岭夏河-合作地区其他岩体的地球化学数据显示的特征一致(图9e, f)。综上可知,早子沟石英闪长玢岩岩浆主要由基性下地壳部分熔融成的。

早子沟石英闪长玢岩锆石$\varepsilon_{Hf}(t)$值为-12.9~-7.2,大多落在球粒陨石均一线之下,对应于重融的古大陆下地壳范围中(图7a, b)。对应的Hf二阶段模式年龄t_{DM}^2为2.10~1.70Ga,主要集中于2.0~1.8Ga。$\varepsilon_{Hf}(t)$变化范围较大,表明源区还有幔源物质的参与(Kemp *et al.*, 2007; Słaby and Martin, 2008)。西秦岭夏河-合作地区早-中三叠世火成岩的锆石Lu-Hf同位素范围集中在-13.0~-3.0,对应的二阶段模式年龄t_{DM}^2为2.10~1.30Ga(骆必继等, 2012; 韦萍等, 2013; Li *et al.*, 2015b; Yu *et al.*, 2022b)。早子沟石英闪长玢岩锆石Lu-Hf同位素与夏河-合作地区花岗质岩体的锆石Lu-Hf同位素值范围近似,表明西秦岭夏河-合作地区早-中三叠世岩浆是古元古代下地壳部分熔融的产物,并有幔源物质的参与。

5.3 对地球动力学背景的约束

西秦岭地区广泛发育的三叠纪火成岩明显与勉略洋壳的俯冲有关(Xiao *et al.*, 2022)。对于西秦岭三叠纪火成岩形成的构造背景目前还存在着巨大争议,一种观点认为形成于活动大陆边缘背景下的勉略洋壳向北俯冲环境(Meng *et al.*, 2005; 张成立等, 2008; Sui *et al.*, 2018; 黄雅琪等, 2020; Wang *et al.*, 2021a);另一种观点则认为形成于与地壳增厚、伸展裂谷等有关的同碰撞至后碰撞环境(李曙光等, 2003; 张宏飞等, 2006; 骆必继等, 2012; Xiong *et al.*, 2018)。总之,西秦岭的构造体系以及勉略洋壳俯冲消亡的确切时间仍不清楚。

目前,对西秦岭早-中三叠纪火成岩形成背景主要存在两种模型:一种模型是板块还未发生碰撞,与勉略洋壳回撤引起的岩石圈地幔流上升有关(Li *et al.*, 2014, 2015b; Qiu *et al.*, 2017; He *et al.*, 2021);另一种是在大陆弧环境到碰撞后伸展的过渡环境中侵位形成的,与板块断离模型有关,形成于勉略洋壳向北俯冲形的大陆弧环境(Lu *et al.*, 1996; Chen and Santosh, 2014; Han *et al.*, 2014)。石英闪长玢岩显示火山弧花岗岩特征,处于华北板块和华南板块碰撞前的构造背景,这与第一种模型相反。西秦岭造山带中具有弧特征的火山岩最早是在晚二叠世石关组沉积岩夹层中的玄武岩中发现的,与俯冲相关的岩浆作用在早-中三叠世达到顶峰(张宏飞等, 2006; Zhang *et al.*, 2007; Li *et al.*, 2014)。西秦岭印支期花岗质岩石沿造山带伸展方向呈线状分布,表现出与岩石圈拆离相反的特征,西秦岭西北部从海相突然转变为陆相,很有可能是大陆碰撞引起的快速隆升和侵蚀,并且黑沟峡MORB型火山岩变质年龄(242~221Ma; Li *et al.*, 1996)也表明勉略洋最早在早三叠世闭合,因此张成立等(2008)认为印支期高钾钙碱性到钾玄质花岗质岩石是在碰撞后环境中形成的。虽然一些早三叠世250~240Ma的高Sr/Y花岗岩显示出增厚地壳部分熔融形成的埃达克岩特征,表现出地壳增厚的构造环境特征(张成立等, 2008; 徐学义等, 2014),但事实上这些高Sr/Y花岗岩的特征与典型埃达克岩的特征不同,这些特征可能来自源岩或表明石榴子石的深部来源(Ren *et al.*, 2018),所以不能通过地壳增厚来解释西秦岭中三叠世花岗岩类的地球化学特征(Dou *et al.*, 2019)。

华北板块和华南板块在三叠纪沿勉略缝合带的碰撞导致了秦岭-大别造山带的叠瓦状逆冲,使地壳增厚达50km(张成立等, 2005)。蛇绿岩套是古缝合带和古俯冲带存在的直接标志,夏河地区存在早二叠世至中二叠世蛇绿混杂岩(Dong *et al.*, 2016);铜仁隆务峡地区蛇绿混杂岩辉长岩的锆石U-Pb年龄为250.1±2.2Ma,以及侵入蛇绿岩的花岗闪长岩的年龄为244.0±1.4Ma(王绘清等, 2010);勉略缝合带中发现了于221~345Ma形成的蛇绿岩(Li *et al.*, 1996; Dong *et al.*, 2021),所以对于勉略洋壳闭合时限仍有争议。但对西秦岭早-中三叠纪一系列花岗质岩体的年代学和岩石地球化学的研究表明,250~230Ma期间勉略洋壳处在俯冲消减阶段(Deng *et al.*, 2021; 李瑞保等, 2018; Qiu *et al.*, 2016b, 2018; Dou *et al.*, 2019; Wang *et al.*, 2021b)。早子沟地区位于西秦岭最西部,在阿尼玛卿-勉略缝合带北侧,石英闪长玢岩侵位时间为~232Ma。它们显示出准铝质-弱过铝质的钙碱性-高钾钙碱性特征,富含LREE,贫HREE,以负Eu异常为特征(图6),具有与火山弧花岗质岩石相同的性质(图10)。在R_1-R_2图解中,石英闪长玢岩落在碰撞前花岗岩区域(图10d),处在活动大陆边缘背景下(图10a)。此外,夏河-合作地区不同岩体的构造图解与石英闪长玢岩相似(图10),表明夏河-合作地区火成岩体在活动大陆边缘背景下形成的,是勉略洋壳向北俯冲南秦岭板块的产物,此时勉略洋壳仍未闭合(图11)。

6 结论

(1)早子沟石英闪长玢岩形成于活动大陆边缘环境,具有碰撞前花岗质岩石特征,侵位于~232Ma,是中三叠世勉略洋壳向北俯冲过程岩浆活动的产物,表明勉略洋壳在~232Ma仍处在俯冲阶段。

(2)石英闪长玢岩为钙碱性-高钾钙碱性岩体,具有较高

$Mg^{\#}$值,$\varepsilon_{Hf}(t)$变化范围较大,由古元古代高钾基性下地壳部分熔融,通过壳幔混染作用与地幔岩浆混合形成。

致谢 感谢俞良军老师对本文的细心审阅;感谢两位匿名审稿人对本文提出的宝贵意见。

References

Allègre CJ and Minster JF. 1978. Quantitative models of trace element behavior in magmatic processes. Earth and Planetary Science Letters, 38(1): 1-25

Andersen T. 2002. Correction of common lead in U-Pb analyses that do not report ^{204}Pb. Chemical Geology, 192(1-2): 59-79

Batchelor RA and Bowden P. 1985. Petrogenetic interpretation of granitoid rock series using multicationic parameters. Chemical Geology, 48(1-4): 43-55

Blatter DL, Sisson TW and Hankins WB. 2013. Crystallization of oxidized, moderately hydrous arc basalt at mid-to lower-crustal pressures: Implications for andesite genesis. Contributions to Mineralogy and Petrology, 166(3): 861-886

Blichert-Toft J and Albarède F. 1997. The Lu-Hf isotope geochemistry of chondrites and the evolution of the mantle-crust system. Earth and Planetary Science Letters, 148(1-2): 243-258

Boynton WV. 1984. Cosmochemistry of the rare earth elements: Meteorite studies. Developments in Geochemistry, 2: 63-114

Cao XF, Lü XB, Yao SZ, Mei W, Zou XY, Chen C, Liu ST, Zhang P, Su YY and Zhang B. 2011. LA-ICP-MS U-Pb zircon geochronology, geochemistry and kinetics of the Wenquan ore-bearing granites from West Qinling, China. Ore Geology Reviews, 43(1): 120-131

Chappell BW and White AJR. 1974. Two contrasting granite types. Pacific Geology, 8: 173-174

Chappell BW. 1999. Aluminium saturation in I- and S-type granites and the characterization of fractionated haplogranites. Lithos, 46(3): 535-551

Chen YJ and Santosh M. 2014. Triassic tectonics and mineral systems in the Qinling Orogen, central China. Geological Journal, 49(4-5): 338-358

Clemens JD, Stevens G and Farina F. 2011. The enigmatic sources of I-type granites: The peritectic connexion. Lithos, 126(3-4): 174-181

Deng J, Wang QF, Li GJ and Santosh M. 2014. Cenozoic tectono-magmatic and metallogenic processes in the Sanjiang region, southwestern China. Earth-Science Reviews, 138: 268-299

Deng J and Wang QF. 2016. Gold mineralization in China: Metallogenic provinces, deposit types and tectonic framework. Gondwana Research, 36: 219-274

Deng J, Wang QF and Li GJ. 2017. Tectonic evolution, superimposed orogeny, and composite metallogenic system in China. Gondwana Research, 50: 216-266

Deng J, Wang CM, Bagas L, Santosh M and Yao EY. 2018. Crustal architecture and metallogenesis in the south-eastern North China Craton. Earth-Science Reviews, 182: 251-272

Deng J, Zhai YS, Mo XX and Wang QF. 2019. Temporal-spatial distribution of metallic ore deposits in China and their geodynamic settings. Society of Economic Geologists Special Publication, 22: 103-132

Deng J, Qiu KF, Wang QF, Goldfarb R, Yang LQ, Zi JW, Geng JZ and Ma Y. 2020a. In situ dating of hydrothermal monazite and implications for the geodynamic controls on ore formation in the Jiaodong gold province, eastern China. Economic Geology, 115(3): 671-685

Deng J, Yang LQ, Groves DI, Zhang L, Qiu KF and Wang QF. 2020b. An integrated mineral system model for the gold deposits of the giant Jiaodong province, eastern China. Earth-Science Reviews, 208: 103274

Deng J, Wang QF, Gao L, He WY, Yang ZY, Zhang SH, Chang LJ, Li GJ, Sun X and Zhou DQ. 2021. Differential crustal rotation and its control on giant ore clusters along the eastern margin of Tibet. Geology, 49(4): 428-432

Deng J, Wang QF, Liu XF, Zhang L, Yang LQ, Yang L, Qiu KF, Guo LN, Liang YY and Ma Y. 2022a. The formation of the Jiaodong gold province. Acta Geologica Sinica, 96(6): 1801-1820

Deng J, Wang QF, Sun X, Yang L, Groves DI, Shu QH, Gao L, Liang LQ, Qiu KF, Wang CM and Dong CY. 2022b. Tibetan ore deposits: A conjunction of accretionary orogeny and continental collision. Earth-Science Reviews, 235: 104245

Di PF. 2018. Geochemistry and ore-forming mechanism on Zaozigou gold deposit in Xiahe-Hezuo, West Qinling, China. Ph. D. Dissertation. Lanzhou: Lanzhou University, 1-96 (in Chinese with English abstract)

Dong YP, Zhang GW, Neubauer F, Liu XM, Genser J and Hauzenberger C. 2011. Tectonic evolution of the Qinling orogen, China: Review and synthesis. Journal of Asian Earth Sciences, 41(3): 213-237

Dong YP and Santosh M. 2016. Tectonic architecture and multiple orogeny of the Qinling Orogenic Belt, Central China. Gondwana Research, 29(1): 1-40

Dong YP, Yang Z, Liu XM, Sun SS, Li W, Cheng B, Zhang FF, Zhang XN, He DF and Zhang GW. 2016. Mesozoic intracontinental orogeny in the Qinling Mountains, central China. Gondwana Research, 30: 144-158

Dong YP, Sun SS, Santosh M, Zhao J, Sun JP, He DF, Shi XH, Hui B, Cheng C and Zhang GW. 2021. Central China Orogenic Belt and amalgamation of East Asian continents. Gondwana Research, 100: 131-194

Dou JZ, Siebel W, He JF and Chen FK. 2019. Different melting conditions and petrogenesis of peraluminous granites in western Qinling, China, and tectonic implications. Lithos, 336-337: 97-111

Douce AEP. 1999. What do experiments tell us about the relative contributions of crust and mantle to the origin of granitic magmas? In: Saunders AD and Norry MJ (eds.). Magmatism in the Ocean Basins. Geological Society, London, Special Publication, 168: 55-75

Elhlou S, Belousova E, Griffin WL, Pearson NJ and O'Reilly SY. 2006. Trace element and isotopic composition of GJ-red zircon standard by laser ablation. Geochimica et Cosmochimica Acta, 70(S18): A158

Frost BR, Barnes CG, Collins WJ, ArCulus RJ, Ellis DJ and Frost CD. 2001. A geochemical classification for granitic rocks. Journal of Petrology, 42(11): 2033-2048

Fu JN, Pirajno F, Yang F, Shivute E, Sun YZ, Ai N and Qiu KF. 2021. Integration of zircon and apatite U-Pb geochronology and geochemical mapping of the Wude basalts (Emeishan large igneous province): A tool for a better understanding of the tectonothermal and geodynamic evolution of the Emeishan LIP. Geoscience Frontiers, 12(2): 573-585

Geng JZ, Huang YQ, Jiang GP, Wu L, Zhu R, Yu HC and Qiu KF. 2019. Zircon U-Pb age and Lu-Hf isotopes of the dacite from Zaozigou Au-Sb deposit, West Qinling, China. Geological Survey and Research, 42(3): 166-173 (in Chinese with English abstract)

Goldfarb RJ, Qiu KF, Deng J, Chen YJ and Yang LQ. 2019. Orogenic gold deposits of China. SEG Special Publications, 22: 263-324

Gorton MP and Schandl ES. 2000. From continents to island arcs: A geochemical index of tectonic setting for arc-related and within-plate felsic to intermediate volcanic rocks. The Canadian Mineralogist, 38(5): 1065-1073

Griffin WL, Wang X, Jackson SE, Pearson NJ, O'Reilly SY, Xu XS and Zhou XM. 2002. Zircon chemistry and magma mixing, SE China: In-situ analysis of Hf isotopes, Tonglu and Pingtan igneous complexes. Lithos, 61(3-4): 237-269

Han JS, Yao JM and Chen YJ. 2014. Geochronology and geochemistry of the Dashui adakitic granitoids in the western Qinling Orogen, central China: Implications for Triassic tectonic setting. Geological Journal, 49(4-5): 383-401

He DY, Qiu KF, Santosh M, Yu HC, Long ZY and Wang JY. 2021. Inhomogeneous crust-mantle interaction and Triassic tectonic escape of a Proterozoic microplate: A tale of the Bikou Terrane. Lithos, 396-397: 106227

Hu FY, Liu SW, Ducea MN, Chapman JB, Wu FY and Kusky T. 2020. Early Mesozoic magmatism and tectonic evolution of the Qinling Orogen: Implications for oblique continental collision. Gondwana Research, 88: 296-332

Hu J, Liu XC, Chen LY, Qu W, Li HK and Geng JZ. 2013. A ~2.5Ga magmatic event at the northern margin of the Yangtze craton: Evidence from U-Pb dating and Hf isotope analysis of zircons from the Douling Complex in the South Qinling orogen. Chinese Science Bulletin, 58(28): 3564-3579

Huang YQ, Qiu KF, Yu HC, Jin DG, He DY, Xiao CH and Wang YX. 2020. Petrogenesis of ore-hosting porphyry in the Gelouang gold deposit, West Qinling and its geological implications. Acta Petrologica Sinica, 36(5): 1567-1585 (in Chinese with English abstract)

Huang YQ, Wu MQ, Germain B, Yu HC, Qiao BX, Zhao ZG and Qiu KF. 2022. Geodynamic setting and ore formation of the Younusisayi thorium deposit in the Altyn orogenic belt, NW China. Ore Geology Reviews, 140: 104552

Jin WJ, Zhang Q, He DF and Jia XQ. 2005. SHRIMP dating of adakites in western Qinling and their implications. Acta Petrologica Sinica, 21(3): 959-966 (in Chinese with English abstract)

Kemp AIS, Hawkesworth CJ, Foster GL, Paterson BA, Woodhead JD, Hergt JM, Gray CM and Whitehouse MJ. 2007. Magmatic and crustal differentiation history of granitic rocks from Hf-O isotopes in zircon. Science, 315(5814): 980-983

Li N, Chen YJ, Santosh M and Pirajno F. 2015a. Compositional polarity of Triassic granitoids in the Qinling Orogen, China: Implication for termination of the northernmost paleo-Tethys. Gondwana Research, 27(1): 244-257

Li RB, Pei XZ, Li ZC, Pei L, Chen GC, Chen YX, Liu CJ and Wang SM. 2018. Paleo-Tethys Ocean subduction in eastern section of East Kunlun Orogen: Evidence from the geochronology and geochemistry of the Wutuo pluton. Acta Petrologica Sinica, 34(11): 3399-3421 (in Chinese with English abstract)

Li SG, Sun WD, Zhang GW, Chen JY and Yang YC. 1996. Chronology and geochemistry of metavolcanic rocks from Heigouxia Valley in the Mian-Lue tectonic zone, South Qinling: Evidence for a Paleozoic oceanic basin and its close time. Science in China (Series D), 39(3): 300-310

Li SG, Hou ZH, Yang YC, Sun WD, Zhang GW and Li QL. 2003. Geochemical characteristics and formation age of Sanchazi ancient magmatic arc in Mianluo Tectonic belt, Southern Qinling Mountains. Science in China (Series D), 33(12): 1163-1173 (in Chinese)

Li SZ, Jahn BM, Zhao SJ, Dai LM, Li XY, Suo YH, Guo LL, Wang YM, Liu XC, Lan HY, Zhou ZZ, Zheng QL and Wang PC. 2017. Triassic southeastward subduction of North China Block to South China Block: Insights from new geological, geophysical and geochemical data. Earth-Science Reviews, 166: 270-285

Li XW, Mo XX, Bader T, Scheltens M, Yu XH, Dong GC and Huang XF. 2014. Petrology, geochemistry and geochronology of the magmatic suite from the Jianzha Complex, central China: Petrogenesis and geodynamic implications. Journal of Asian Earth Sciences, 95: 164-181

Li XW, Mo XX, Huang XF, Dong GC, Yu XH, Luo MF and Liu YB. 2015b. U-Pb zircon geochronology, geochemical and Sr-Nd-Hf isotopic compositions of the Early Indosinian Tongren pluton in West Qinling: Petrogenesis and geodynamic implications. Journal of Asian Earth Sciences, 97: 38-50

Liang ZL, Chen GZ, Ma HS and Zhang YN. 2016. Evolution of ore-controlling faults in the Zaozigou gold deposit, western Qinling. Geotectonica et Metallogenia, 40(2): 354-366 (in Chinese with English abstract)

Liu L, Liao XY, Wang YW, Wang C, Santosh M, Yang M, Zhang CL and Chen DL. 2016. Early Paleozoic tectonic evolution of the North Qinling Orogenic Belt in Central China: Insights on continental deep subduction and multiphase exhumation. Earth-Science Reviews, 159: 58-81

Liu Y, Liu, YH, Dong FC, Li ZH, Yu JK and Ma XP. 2012. Accurate dating of mineralogenetic epoch and its geological significance in Zaozigou gold deposit, Gansu Province. Gold, 33(11): 10-17 (in Chinese with English abstract)

Liu YS, Hu ZC, Zong KQ, Gao CG, Gao S, Xu J and Chen HH. 2010. Reappraisement and refinement of zircon U-Pb isotope and trace element analyses by LA-ICP-MS. Chinese Science Bulletin, 55(15): 1535-1546

Lu XX, Dong Y, Chang QL, Xiao QH, Li XB, Wang XX and Zhang GW. 1996. Indosinian Shahewan rapakivi granite in Qinling and its dynamic significance. Science in China (Series D), 39(3): 266-272

Ludwig KR. 2003. ISOPLOT 3.00: A Geochronological Toolkit for Microsoft Excel. Berkeley: Berkeley Geochronology Center

Luo BJ, Zhang HF and Lü XB. 2012. U-Pb zircon dating, geochemical and Sr-Nd-Hf isotopic compositions of Early Indosinian intrusive rocks in West Qinling, central China: Petrogenesis and tectonic implications. Contributions to Mineralogy and Petrology, 164(4): 551-569

Luo BJ, Zhang HF and Xiao ZQ. 2012. Petrogenesis and tectonic implications of the Early Indosinian Meiwu pluton in West Qinling, central China. Earth Science Frontiers, 19(3): 199-213 (in Chinese with English abstract)

Luo BJ. 2013. Petrogenesis and geodynamic processes of the Indosinian magmatism in the west Qinling orogenic belt, central China. Ph. D. Dissertation. Wuhan: China University of Geosciences, 1-191 (in Chinese with English abstract)

Luo BJ, Zhang HF, Xu WC, Guo L, Pan FB and Yang H. 2015. The Middle Triassic Meiwu batholith, West Qinling, Central China: Implications for the evolution of compositional diversity in a composite batholith. Journal of Petrology, 56(6): 1139-1172

Mao JW, Qiu YM, Goldfarb RJ, Zhang ZC, Garwin S and Ren FS. 2002. Geology, distribution, and classification of gold deposits in the western Qinling belt, central China. Mineralium Deposita, 37(3-4): 352-377

Meng QR and Zhang GW. 2000. Geologic framework and tectonic evolution of the Qinling orogen, central China. Tectonophysics, 323(3-4): 183-196

Meng QR, Wang E and Hu JM. 2005. Mesozoic sedimentary evolution of the Northwest Sichuan basin: Implication for continued clockwise rotation of the South China block. GSA Bulletin, 117(3-4): 396-410

Middlemost EAK. 1994. Naming materials in the magma/igneous rock system. Earth-Science Reviews, 37(3-4): 215-224

Miller C, Schuster R, Klötzli U, Frank W and Purtscheller F. 1999. Post-collisional potassic and ultrapotassic magmatism in SW Tibet: Geochemical and Sr-Nd-Pb-O isotopic constraints for mantle source characteristics and petrogenesis. Journal of Petrology, 40(9): 1399-1424

Moyen JF. 2009. High Sr/Y and La/Yb ratios: The meaning of the "adakitic signature". Lithos, 112(3-4): 556-574

Nandedkar RH, Ulmer P and Müntener O. 2014. Fractional crystallization of primitive, hydrous arc magmas: An experimental study at 0.7GPa. Contributions to Mineralogy and Petrology, 167(6): 1015

Pearce JA, Harris NBW and Tindle AG. 1984. Trace element discrimination diagrams for the tectonic interpretation of granitic rocks. Journal of Petrology, 25(4): 956-983

Pei XZ, Ding SP, Li ZC, Liu ZQ, Li ZB, Feng JY, Sun Y, Zhang YF, Liu ZG, Zhang XF, Chen GC and Chen YX. 2009. Early Paleozoic Tianshui-Wushan tectonic zone of the northern margin of West Qinling and its tectonic evolution. Acta Geologica Sinica, 83(11):

1547 – 1564 (in Chinese with English abstract)

Qiu KF, Deng J, Taylor RD, Song KR, Song YH, Li QZ and Goldfarb RJ. 2016a. Paleozoic magmatism and porphyry Cu-mineralization in an evolving tectonic setting in the North Qilian Orogenic Belt, NW China. Journal of Asian Earth Sciences, 122: 20 – 40

Qiu KF, Taylor RD, Song YH, Yu HC, Song KR and Li N. 2016b. Geologic and geochemical insights into the formation of the Taiyangshan porphyry copper-molybdenum deposit, Western Qinling Orogenic Belt, China. Gondwana Research, 35: 40 – 58

Qiu KF and Deng J. 2017. Petrogenesis of granitoids in the Dewulu skarn copper deposit: Implications for the evolution of the Paleotethys Ocean and mineralization in western Qinling, China. Ore Geology Reviews, 90: 1078 – 1098

Qiu KF, Marsh E, Yu HC, Pfaff K, Gulbransen C, Gou ZY and Li N. 2017. Fluid and metal sources of the Wenquan porphyry molybdenum deposit, western Qinling, NW China. Ore Geology Reviews, 86: 459 – 473

Qiu KF, Yu HC, Gou ZY, Liang ZL, Zhang JL and Zhu R. 2018. Nature and origin of Triassic igneous activity in the Western Qinling Orogen: The Wenquan composite pluton example. International Geology Review, 60(2): 242 – 266

Qiu KF, Yu HC, Wu MQ, Geng JZ, Ge XK, Gou ZY and Taylor RD. 2019. Discrete Zr and REE mineralization of the Baerzhe rare-metal deposit, China. American Mineralogist, 104(10): 1487 – 1502

Qiu KF, Yu HC, Deng J, McIntire D, Gou ZY, Geng JZ, Chang ZS, Zhu R, Li KN and Goldfarb R. 2020. The giant Zaozigou Au-Sb deposit in West Qinling, China: Magmatic- or metamorphic-hydrothermal origin? Mineralium Deposita, 55(2): 345 – 362

Qiu KF, Deng J, Yu HC, Wu MQ, Wang Y, Zhang L and Goldfarb R. 2021a. Identifying hydrothermal quartz vein generations in the Taiyangshan porphyry Cu-Mo deposit (West Qinling, China) using cathodoluminescence, trace element geochemistry, and fluid inclusions. Ore Geology Reviews, 128: 103882

Qiu KF, Yu HC, Hetherington C, Huang YQ, Yang T and Deng J. 2021b. Tourmaline composition and boron isotope signature as a tracer of magmatic-hydrothermal processes. American Mineralogist, 106(7): 1033 – 1044

Qiu KF, Deng J, Sai SX, Yu HC, Tamer MT, Ding ZJ, Yu XF and Goldfarb RJ. 2023a. Low-temperature thermochronology for defining the tectonic controls on heterogeneous gold endowment across the Jiaodong Peninsula, eastern China. Tectonics, 42(1): e2022TC007669

Qiu KF, Deng J, Laflamme C, Long ZY, Wan RQ, Moynier F, Yu HC, Zhang JY, Ding ZJ and Goldfarb RJ. 2023b. Giant Mesozoic gold ores derived from subducted oceanic slab and overlying sediments. Geochimica et Cosmochimica Acta, 343(15): 133 – 141

Rapp RP and Watson EB. 1995. Dehydration melting of metabasalt at 8 ~ 32kbar: Implications for continental growth and crust-mantle recycling. Journal of Petrology, 36(4): 891 – 931

Ren L, Liang HY, Bao ZW, Zhang J, Li KX and Huang WT. 2018. Genesis of the high Sr/Y rocks in Qinling orogenic belt, Central China. Lithos, 314 – 315: 337 – 349

Roden MF and Shimizu N. 2000. Trace element abundances in mantle-derived minerals which bear on compositional complexities in the lithosphere of the Colorado Plateau. Chemical Geology, 165(3 – 4): 283 – 305

Shi Y, Yu JH, Xu XS, Tang HF, Qiu JS and Chen LH. 2011. U-Pb ages and Hf isotope compositions of zircons of Taihua Group in Xiaoqinling area, Shaanxi Province. Acta Petrologica Sinica, 27(10): 3095 – 3108 (in Chinese with English abstract)

Sisson TW, Ratajeski K, Hankins WB and Glazner AF. 2005. Voluminous granitic magmas from common basaltic sources. Contributions to Mineralogy and Petrology, 148(6): 635 – 661

Skjerlie KP and Johnston AD. 1993. Fluid-absent melting behavior of an F-rich tonalitic gneiss at mid-crustal pressures: Implications for the generation of anorogenic granites. Journal of Petrology, 34(4): 785 – 815

Słaby E and Martin H. 2008. Mafic and felsic magma interaction in granites: The Hercynian Karkonosze Pluton (Sudetes, Bohemian Massif). Journal of Petrology, 49(2): 353 – 391

Soesoo A. 2000. Fractional crystallization of mantle-derived melts as a mechanism for some I-type granite petrogenesis: An example from Lachlan Fold Belt, Australia. Journal of the Geological Society, 157(1): 135 – 149

Sui JX and Li JW. 2013. Geochronology and genesis of the Zaozigou gold deposit, Xiahe-Hezuo district, West Qinling. Acta Mineralogica Sinica, 33(Suppl.2): 346 – 347 (in Chinese)

Sui JX, Li JW, Wen G and Jin XY. 2017. The Dewulu reduced Au-Cu skarn deposit in the Xiahe-Hezuo district, West Qinling orogen, China: Implications for an intrusion-related gold system. Ore Geology Reviews, 80: 1230 – 1244

Sui JX, Li JW, Jin XY, Vasconcelos P and Zhu R. 2018. $^{40}Ar/^{39}Ar$ and U-Pb constraints on the age of the Zaozigou gold deposit, Xiahe-Hezuo district, West Qinling orogen, China: Relation to Early Triassic reduced intrusions emplaced during slab rollback. Ore Geology Reviews, 101: 885 – 899

Sun SS and McDonough WF. 1989. Chemical and isotopic systematics of oceanic basalts: Implications for mantle composition and processes. In: Saunders AD and Norry MJ (eds.). Magmatism in the Ocean Basins. Geological Society, London, Special Publication, 42(1): 313 – 345

Wang HQ, Zhu YH, Lin QX, Li YL and Wang K. 2010. LA-ICP-MS zircon U-Pb dating of the gabbro from Longwu gorge ophiolite, Jianzha-Tongren area, Qinghai, China and its geological significance. Geological Bulletin of China, 29(1): 86 – 92 (in Chinese with English abstract)

Wang J, Yu HC, He DY, Sun W, Wang YX, Liu PX and Qiu KF. 2021a. Geochronology and geochemistry of the Yidi'nan quartz diorite in the West Qinling, China: Implications for evolution of the Palaeo-Tethys Ocean. Geological Journal, 56(4): 2277 – 2295

Wang M, Pei XZ, Li ZC, Li RB, Pei L, Chen YX, Liu CJ, Zhao SW, Chen GC and Gao F. 2021b. Genesis of Middle Triassic high-$Mg^{\#}$ quartz diorites from the Xiahe area, West Qinling Orogen, Central China, and their geodynamic implications. Journal of Geodynamics, 143: 101805

Wang QF, Yang L, Xu XJ, Santosh M, Wang YN, Wang TY, Chen FG, Wang RX, Gao L, Liu XF, Yang SJ, Zeng YS, Chen JH, Zhang QZ and Deng J. 2020. Multi-stage tectonics and metallogeny associated with Phanerozoic evolution of the South China Block: A holistic perspective from the Youjiang Basin. Earth-Science Reviews, 211: 103405

Wei LX, Chen ZL, Pang ZS, Han FB and Xiao CH. 2018. An analysis of the tectonic stress field in the Zaozigou gold deposit, Hezuo area, Gansu Province. Acta Geoscientica Sinica, 39(1): 79 – 93 (in Chinese with English abstract)

Wei P, Mo XX, Yu XH, Huang XF, Ding Y and Li XW. 2013. Geochemistry, chronology and geological significance of the granitoids in Xiahe, West Qinling. Acta Petrologica Sinica, 29(11): 3981 – 3992 (in Chinese with English abstract)

Wu FY, Li XH, Zheng YF and Gao S. 2007. Lu-Hf isotopic systematics and their applications in petrology. Acta Petrologica Sinica, 23(2): 185 – 220 (in Chinese with English abstract)

Wu K, Ling MX, Hu YB, Guo J, Jiang XY, Sun SJ, Liang HY, Liu X and Sun WD. 2018. Melt-fluxed melting of the heterogeneously mixed lower arc crust: A case study from the Qinling orogenic belt, Central China. Geochemistry, Geophysics, Geosystems, 19(6): 1767 – 1788

Wu MQ, Samon IM, Qiu KF and Zhang DH. 2022. Multi-stage metasomatic Zr mineralization in the world-class Baerzhe rare earth element Nb-Zr-Be deposit, China. American Mineralogist, 108(2): 389 – 405

Xiao B, Li QG, Liu SW, Wang ZQ, Yang PT, Chen JL and Xu XY. 2014. Highly fractionated Late Triassic I-type granites and related molybdenum mineralization in the Qinling orogenic belt: Geochemical and U-Pb-Hf and Re-Os isotope constraints. Ore Geology Reviews, 56: 220 – 233

Xiao CH, Chen ZL, Han FB, Wei LX and Ma LT. 2022. Provenance and tectonic significance of Lower Triassic clastic sedimentary rocks of the West Qinling Orogenic Belt, Central China. Journal of Asian Earth Sciences, 224: 105026

Xiong X, Zhu LM, Zhang GW, Li B, Qi L, Stevenson D, Yang T, Wang F, Zheng J, Jiang H and Guo AL. 2016. Geology and geochemistry of the Triassic Wenquan Mo deposit and Mo-mineralized granite in the Western Qinling Orogen, China. Gondwana Research, 30: 159 – 178

Xiong X, Zhu LM, Zhang GW, Li N, Yuan HL, Ding LL, Sun C and Guo AL. 2018. Fluid inclusion geochemistry and magmatic oxygen fugacity of the Wenquan Triassic molybdenum deposit in the Western Qinling Orogen, China. Ore Geology Reviews, 99: 244 – 263

Xu XY, Chen JL, Gao T, Li P and Li T. 2014. Granitoid magmatism and tectonic evolution in northern edge of the western Qinling terrane. Acta Petrologica Sinica, 30(2): 371 – 389 (in Chinese with English abstract)

Yang HW. 2018. Geochemical, geochronology, and tectonic significance of Triassic Meiwu pluton in the western Qinling Orogen. Master Degree Thesis. Beijing: China University of Geosciences (Beijing), 1 – 85 (in Chinese with English abstract)

Yang L, Wang QF, Large RR, Fougerouse D, Mukherjee I, Zhang QZ, and Deng J. 2022. Texture and geochemistry of pyrite from the Jinya, Nakuang and Gaolong gold deposits in the Youjiang Basin: implications for basin-scale gold mineralization. Mineralium Deposita, 57(8): 1367 – 1390

Yang LQ, Deng J, Qiu KF, Ji XZ, Santosh M, Song KR, Song YH, Geng JZ, Zhang C and Hua B. 2015a. Magma mixing and crust-mantle interaction in the Triassic monzogranites of Bikou Terrane, central China: Constraints from petrology, geochemistry, and zircon U-Pb-Hf isotopic systematics. Journal of Asian Earth Sciences, 98: 320 – 341

Yang LQ, Deng J, Dilek Y, Qiu KF, Ji XZ, Li N, Taylor RD and Yu JY. 2015b. Structure, geochronology, and petrogenesis of the Late Triassic Puziba granitoid dikes in the Mianlue suture zone, Qinling orogen, China. GSA Bulletin, 127(11 – 12): 1831 – 1854

Yang LQ, Deng J, Li N, Zhang C, Ji XZ and Yu JY. 2016a. Isotopic characteristics of gold deposits in the Yangshan Gold Belt, West Qinling, central China: Implications for fluid and metal sources and ore genesis. Journal of Geochemical Exploration, 168: 103 – 118

Yang LQ, Deng J, Wang ZL, Guo LN, Li RH, Groves DI, Danyushevsky LV, Zhang C, Zheng XL and Zhao H. 2016b. Relationships between gold and pyrite at the Xincheng gold deposit, Jiaodong Peninsula, China: Implications for gold source and deposition in a brittle epizonal environment. Economic Geology, 111(1): 105 – 126

Yu HC, Guo CA, Qiu KF, Mcintire D, Jiang GP, Gou ZY, Geng JZ, Pang Y, Zhu R and Li NB. 2019. Geochronological and geochemical constraints on the formation of the giant Zaozigou Au-Sb deposit, West Qinling, China. Minerals, 9(1): 37

Yu HC, Qiu KF, Nassif MT, Geng JZ, Sai SX, Duo DW, Huang YQ and Wang J. 2020a. Early orogenic gold mineralization event in the West Qinling related to closure of the Paleo-Tethys Ocean-Constraints from the Ludousou gold deposit, central China. Ore Geology Reviews, 117: 103217

Yu HC, Qiu KF, Sai SX, Mcintire DC, Pirajno F, Duo DW, Miggins DP, Wang J, Jia RY and Wu MQ. 2020b. Paleo-Tethys Late Triassic orogenic gold mineralization recorded by the Yidi'nan gold deposit, West Qinling, China. Ore Geology Reviews, 116: 103211

Yu HC, Qiu KF, Hetherington CJ, Chew D, Huang YQ, He DY, Geng JZ and Xian HY. 2021. Apatite as an alternative petrochronometer to trace the evolution of magmatic systems containing metamict zircon. Contributions to Mineralogy and Petrology, 176(9): 68

Yu HC, Qiu KF, Deng J, Zhu R, Mathieu L, Sai SX and Sha WJ. 2022a. Exhuming and preserving epizonal orogenic Au-Sb deposits in rapidly uplifting orogenic settings. Tectonics, 41(8): e2021TC007165

Yu HC, Qiu KF, Pirajno F, Zhang PC and Dong WQ. 2022b. Revisiting Phanerozoic evolution of the Qinling Orogen (East Tethys) with perspectives of detrital zircon. Gondwana Research, 103: 426 – 444

Zhang CL, Zhang GW, Yan YX and Wang Y. 2005. Origin and dynamic significance of Guangtoushan granitic plutons to the north of Mianlue zone in southern Qinling. Acta Petrologica Sinica, 21(3): 711 – 720 (in Chinese with English abstract)

Zhang CL, Wang T and Wang XX. 2008. Origin and tectonic setting of the Early Mesozoic granitoids in Qinling orogenic belt. Geological Journal of China Universities, 14(3): 304 – 316 (in Chinese with English abstract)

Zhang GW, Meng QR, Yu ZP, Sun Y, Zhou DW and Guo AL. 1996. Orogenic process and dynamic characteristics of Qinling Orogenic belt. Science in China (Series D), 26(3): 193 – 200 (in Chinese)

Zhang GW, Zhang BR, Yuan XC and Xiao QH. 2001. Qinling Orogenic Beit and Continental Dynamics. Beijing: Science Press, 1 – 855 (in Chinese)

Zhang HF, Chen YL, Xu WC, Liu R, Yuan HL and Liu XM. 2006. Granitoids around Gonghe basin in Qinghai Province: Petrogenesis and tectonic implications. Acta Petrologica Sinica, 22(12): 2910 – 2922 (in Chinese with English abstract)

Zhang HF, Jin LL, Zhang L, Harris N, Zhou L, Hu SH and Zhang BR. 2007. Geochemical and Pb-Sr-Nd isotopic compositions of granitoids from western Qinling belt: Constraints on basement nature and tectonic affinity. Science in China (Series D), 50(2): 184 – 196

Zhang L, Qiu KF, Hou ZL, Pirajno F, Shivute E and Cai YW. 2021. Fluid-rock reactions of the Triassic Taiyangshan porphyry Cu-Mo deposit (West Qinling, China) constrained by QEMSCAN and iron isotope. Ore Geology Reviews, 132: 104068

Zhao TP, Zhai MG, Xia B, Li HM, Zhang YX and Wan YS. 2004. Zircon U-Pb SHRIMP dating for the volcanic rocks of the Xiong'er Group: Constraints on the initial formation age of the cover of the North China Craton. Chinese Science Bulletin, 49(23): 2495 – 2502

Zheng YF, Zhao ZF, Wu YB, Zhang SB, Liu XM and Wu FY. 2006. Zircon U-Pb age, Hf and O isotope constraints on protolith origin of ultrahigh-pressure eclogite and gneiss in the Dabie orogen. Chemical Geology, 231(1 – 2): 135 – 158

Zhu LM, Zhang GW, Chen YJ, Ding ZJ, Guo B, Wang F and Lee B. 2011. Zircon U-Pb ages and geochemistry of the Wenquan Mo-bearing granitioids in West Qinling, China: Constraints on the geodynamic setting for the newly discovered Wenquan Mo deposit. Ore Geology Reviews, 39(1 – 2): 46 – 62

Zhu LM, Zhang GW, Yang T, Wang F and Gong HJ. 2013. Geochronology, petrogenesis and tectonic implications of the Zhongchuan granitic pluton in the Western Qinling metallogenic belt, China. Geological Journal, 48(4): 310 – 334

Zou FH, Wu CL, Deng LH, Gao D and Gao YH. 2022. Petrological and geochemical constraints on the petrogenesis of granitoids in the Gonghe geothermal basin, western Qinling (China). Applied Geochemistry, 136: 105176

附中文参考文献

第鹏飞. 2018. 西秦岭夏河-合作早子沟金矿床地球化学特征及成矿机制研究. 博士学位论文. 兰州：兰州大学，1 – 96

耿建珍，黄雅琪，姜桂鹏，吴磊，朱锐，于皓丞，邱昆峰. 2019. 西秦岭早子沟金锑矿床含矿英安斑岩年代学及其成因. 地质调查与研究，42(3)：166 – 173

黄雅琪，邱昆峰，于皓丞，金鼎国，何登洋，肖昌浩，王玉玺. 2020. 西秦岭格娄昂金矿床赋矿斑岩岩石成因及其地质意义. 岩石学报，36(5)：1567 – 1585

金维浚，张旗，何登发，贾秀勤. 2005. 西秦岭埃达克岩的 SHRIMP 定年及其构造意义. 岩石学报，21(3)：959 – 966

李瑞保，裴先治，李佐臣，裴磊，陈国超，陈有炘，刘成军，王生明．2018．东昆仑东段古特提斯洋俯冲作用——乌妥花岗岩体锆石 U-Pb 年代学和地球化学证据．岩石学报，34(11)：3399－3421

李曙光，侯振辉，杨永成，孙卫东，张国伟，李秋立．2003．南秦岭勉略构造带三岔子古岩浆弧的地球化学特征及形成时代．中国科学(D 辑)，33(12)：1163－1173

梁志录，陈国忠，麻红顺，张愿宁．2016．西秦岭早子沟金矿控矿断裂形成演化．大地构造与成矿学，40(2)：354－366

刘勇，刘云华，董福辰，李中会，于建坤，马晓平．2012．甘肃枣子沟金矿床成矿时代精确测定及其地质意义．黄金，33(11)：10－17

骆必继，张宏飞，肖尊奇．2012．西秦岭印支早期美武岩体的岩石成因及其构造意义．地学前缘，19(3)：199－213

骆必继．2013．西秦岭造山带印支期岩浆作用及深部过程．博士学位论文．武汉：中国地质大学，1－191

裴先治，丁仨平，李佐臣，刘战庆，李瑞保，冯建赟，孙雨，张亚峰，刘智刚，张晓飞，陈国超，陈有炘．2009．西秦岭北缘早古生代天水-武山构造带及其构造演化．地质学报，83(11)：1547－1564

时毓，于津海，徐夕生，唐红峰，邱检生，陈立辉．2011．陕西小秦岭地区太华群的锆石 U-Pb 年龄和 Hf 同位素组成．岩石学报，27(10)：3095－3108

隋吉祥，李建威．2013．西秦岭夏河-合作地区枣子沟金矿床成矿时代与矿床成因．矿物学报，33(增2)：346－347

王绘清，朱云海，林启祥，李益龙，王坤．2010．青海尖扎-同仁地区隆务峡蛇绿岩的形成时代及意义——来自辉长岩锆石 LA-ICP-MS U-Pb 年龄的证据．地质通报，29(1)：86－92

韦良喜，陈正乐，庞振山，韩风彬，肖昌浩．2018．甘肃省合作市早子沟金矿床构造应力场分析．地球学报，39(1)：79－93

韦萍，莫宣学，喻学惠，黄雄飞，丁一，李小伟．2013．西秦岭夏河花岗岩的地球化学、年代学及地质意义．岩石学报，29(11)：3981－3992

吴福元，李献华，郑永飞，高山．2007．Lu-Hf 同位素体系及其岩石学应用．岩石学报，23(2)：185－220

徐学义，陈隽璐，高婷，李平，李婷．2014．西秦岭北缘花岗质岩浆作用及构造演化．岩石学报，30(2)：371－389

杨瀚文．2018．西秦岭美武一带三叠纪岩体的岩石地球化学、年代学及其地质意义．硕士学位论文．北京：中国地质大学(北京)，1－85

张成立，张国伟，晏云翔，王煜．2005．南秦岭勉略带北光头山花岗岩体群的成因及其构造意义．岩石学报，21(3)：711－720

张成立，王涛，王晓霞．2008．秦岭造山带早中生代花岗岩成因及其构造环境．高校地质学报，14(3)：304－316

张国伟，孟庆任，于在平，孙勇，周鼎武，郭安林．1996．秦岭造山带的造山过程及其动力学特征．中国科学(D 辑)，26(3)：193－200

张国伟，张本仁，袁学诚，肖庆辉．2001．秦岭造山带与大陆动力学．北京：科学出版社，1－855

张宏飞，陈岳龙，徐旺春，刘荣，袁洪林，柳小明．2006．青海共和盆地周缘印支期花岗岩类的成因及其构造意义．岩石学报，22(12)：2910－2922